

1
2
3
4
5
6
7
8
9
10
11
12
13
14
15
16
17
18
19
20
21
22

Dystroglycan N-terminal domain enables LARGE1 to extend matriglycan on α -dystroglycan and prevents muscular dystrophy

**Hidehiko Okuma¹, Jeffrey M. Hord¹, Ishita Chandel¹, David Venzke¹, Mary E. Anderson¹,
Ameya S. Walimbe¹, Soumya Joseph¹, Zeita Gastel¹, Yuji Hara², Fumiaki Saito³,
Kiichiro Matsumura³, and Kevin P. Campbell^{1*}**

¹Howard Hughes Medical Institute, Senator Paul D. Wellstone Muscular Dystrophy Specialized Research Center, Department of Molecular Physiology and Biophysics and Department of Neurology, Roy J. and Lucille A. Carver College of Medicine, The University of Iowa, Iowa City, Iowa 52242, USA

²Department Pharmaceutical Sciences, School of Pharmaceutical Sciences, University of Shizuoka, Shizuoka 4228526, Japan

³Department of Neurology, School of Medicine, Teikyo University, Tokyo 1738606, Japan

* Corresponding author

23 **Abstract**

24 Dystroglycan (DG) requires extensive post-translational processing to function as a
25 receptor for extracellular matrix proteins containing laminin-G-like (LG) domains. Matriglycan
26 is an elongated polysaccharide of alternating xylose and glucuronic acid that is uniquely
27 synthesized on α -dystroglycan (α -DG) by like-acetylglucosaminyltransferase-1 (LARGE1) and
28 binds with high affinity to matrix proteins like laminin. Defects in the post-translational
29 processing of α -DG that result in a shorter form of matriglycan reduce the size of α -DG and
30 decrease laminin binding, leading to various forms of muscular dystrophy. However, little is
31 known regarding mechanisms that generate full-length matriglycan on α -DG (~150-250 kDa).
32 Here, we show that LARGE1 can only synthesize a short, non-elongated form of matriglycan in
33 mouse skeletal muscle that lacks the DG N-terminus (α -DGN), resulting in a ~100-125 kDa α -
34 DG. This smaller form of α -DG binds laminin and maintains specific force but does not prevent
35 muscle pathophysiology, including reduced force induced by eccentric contractions and
36 abnormalities in neuromuscular junctions. Collectively, our study demonstrates that α -DGN is
37 required for LARGE1 to extend matriglycan to its full mature length on α -DG and thus prevent
38 muscle pathophysiology.

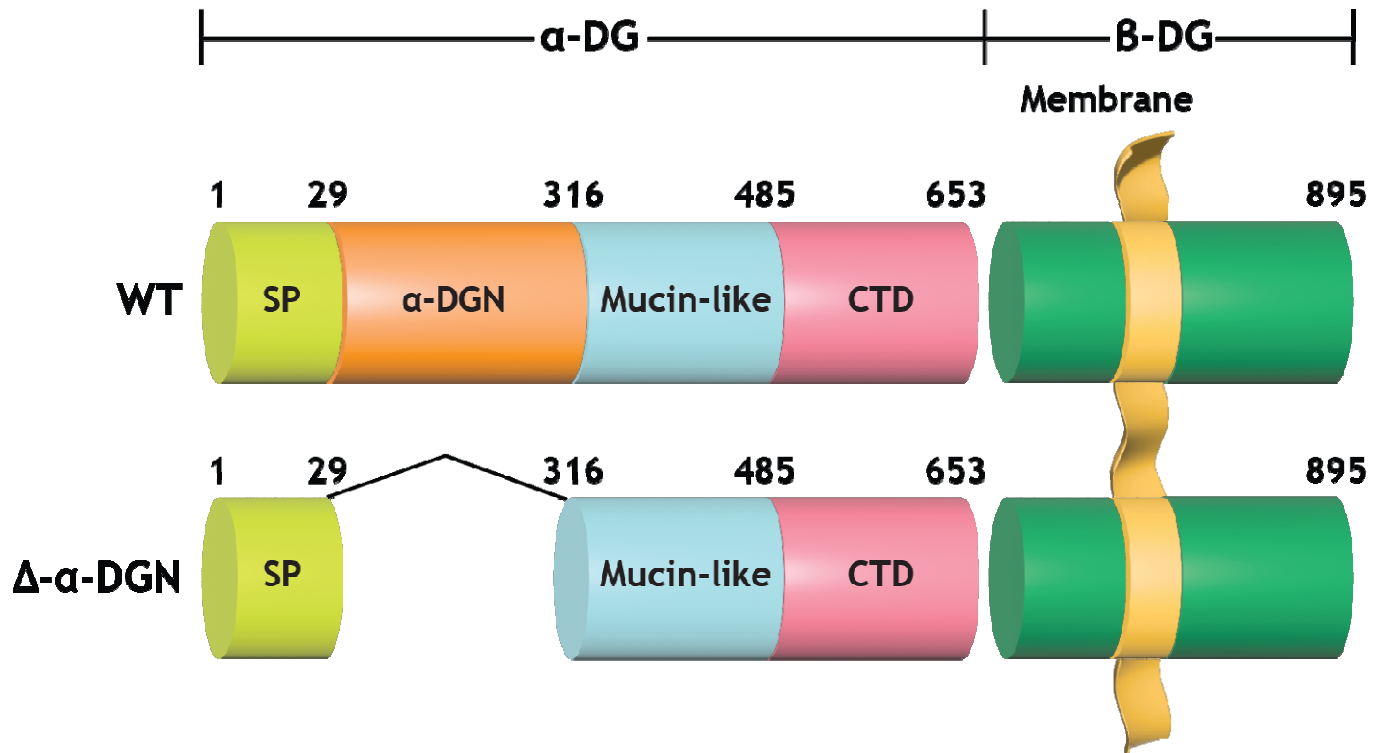
39 Introduction

40 The basement membrane is a specialized network of extracellular matrix macromolecules
41 that surrounds epithelium, endothelium, muscle, fat, and neurons (*Rowe and Weiss, 2008*).
42 Skeletal muscle cells are bound to the basement membrane through transmembrane receptors,
43 including dystroglycan (DG) and the integrins, which help maintain the structural and functional
44 integrity of the muscle cell membrane (*Roberts et al., 1985; Sonnenberg et al., 1988;*
45 *Ibraghimov-Beskrovnaya et al., 1992; Han et al., 2009*). DG is a central component of the
46 dystrophin-glycoprotein complex (DGC). It is encoded by a single gene, DAG1, and cleaved into
47 α - and β -subunits (α -DG and β -DG, respectively) by post-translational processing (*Ibraghimov-*
48 *Beskrovnaya et al., 1992*). Extensive O-glycosylation of α -dystroglycan (α -DG) is required for
49 normal muscle function, and defects in this process result in various forms of muscular
50 dystrophy. (*Michele et al., 2002; Yoshida-Moriguchi and Campbell, 2015*)

51 α -DG binds to ECM ligands containing laminin-G domains (e.g., laminin, agrin,
52 perlecan) that are essential components of the basement membrane (*Michele et al., 2002*). DG,
53 therefore, physically links the cell membrane to the basement membrane. This process requires
54 synthesis of matriglycan, a heteropolysaccharide [-GlcA- β 1,3-Xyl- α 1,3-]_n, on α -DG by the
55 bifunctional glycosyltransferase, like-acetylglucosaminyltransferase-1 (LARGE1) (*Chiba et al.,*
56 *1997; Michele et al., 2002; Inamori et al., 2012; Yoshida-Moriguchi and Campbell, 2015;*
57 *Hohenester, 2019; Michele et al., 2002; Ohtsubo and Marth, 2006*). O-glycosylation and the
58 glycosylation-specific kinase, Protein O-Mannose Kinase (POMK), which phosphorylates
59 mannose of the core M3 trisaccharide (GalNAc- β 1,3-GlcNAc- β 1,4-Man), are required to
60 produce full-length, high-molecular weight forms of matriglycan (*Yoshida-Moriguchi and*
61 *Campbell, 2015; Hohenester, 2019; Jae et al., 2013; Yoshida-Moriguchi et al., 2013; Zhu et*
62 *al., 2016*). In the absence of phosphorylation of core M3 by POMK, LARGE1 synthesizes a

63 short, non-elongated form of matriglycan on α -DG (*Walimbe et al., 2020*). Notably, a loss of
64 function in the post-translational addition of matriglycan causes dystroglycanopathies, which are
65 congenital and limb-girdle muscular dystrophies with or without brain and eye abnormalities.
66 Disease severity is dependent on the ability of matriglycan to bind ECM ligands, which is
67 dictated by its length and expression (*Goddeeris et al., 2013*): matriglycan that is low molecular
68 weight (e.g., short) can cause muscular dystrophy, even if its capacity to bind laminin-G domains
69 is not completely lost (*Puckett et al., 2009; Hara et al., 2011; Carss et al., 2013; Cirak et al.,*
70 *2013; Dong et al., 2015; Walimbe et al., 2020*). However, the regulation of matriglycan
71 elongation by factors other than POMK is still unknown.

72 α -DG is composed of three distinct domains: the N-terminal (α -DGN) domain, a central
73 mucin-like domain, and the C-terminal domain (*Figure 1*) (*Brancaccio et al., 1995*). α -DGN
74 functions as a binding site for LARGE1 in the Golgi and is required for the functional
75 glycosylation of the mucin-like domain of α -DG (*Kanagawa et al., 2004*). Therefore, we
76 hypothesized that α -DGN must be involved in regulating the production and elongation of
77 matriglycan. Here, we used a multidisciplinary approach to show that LARGE1 synthesizes a
78 non-elongated form of matriglycan on DG that lacks α -DGN (i.e., α -DGN-deleted dystroglycan)
79 resulting in ~100-125 kDa α -DG. This short form of matriglycan binds laminin and maintains
80 muscle-specific force. However, it fails to prevent lengthening contraction-induced reduction in
81 force, neuromuscular junction abnormalities, or dystrophic changes in muscle, as these effects
82 require the expression of α -DG with the matriglycan modification that is at least 150 kDa.
83 Therefore, this study shows that LARGE1 requires α -DGN to generate full-length (~150-250
84 kDa) matriglycan in skeletal muscle, but synthesis of a shorter form of matriglycan still occurs in
85 the absence of this domain.



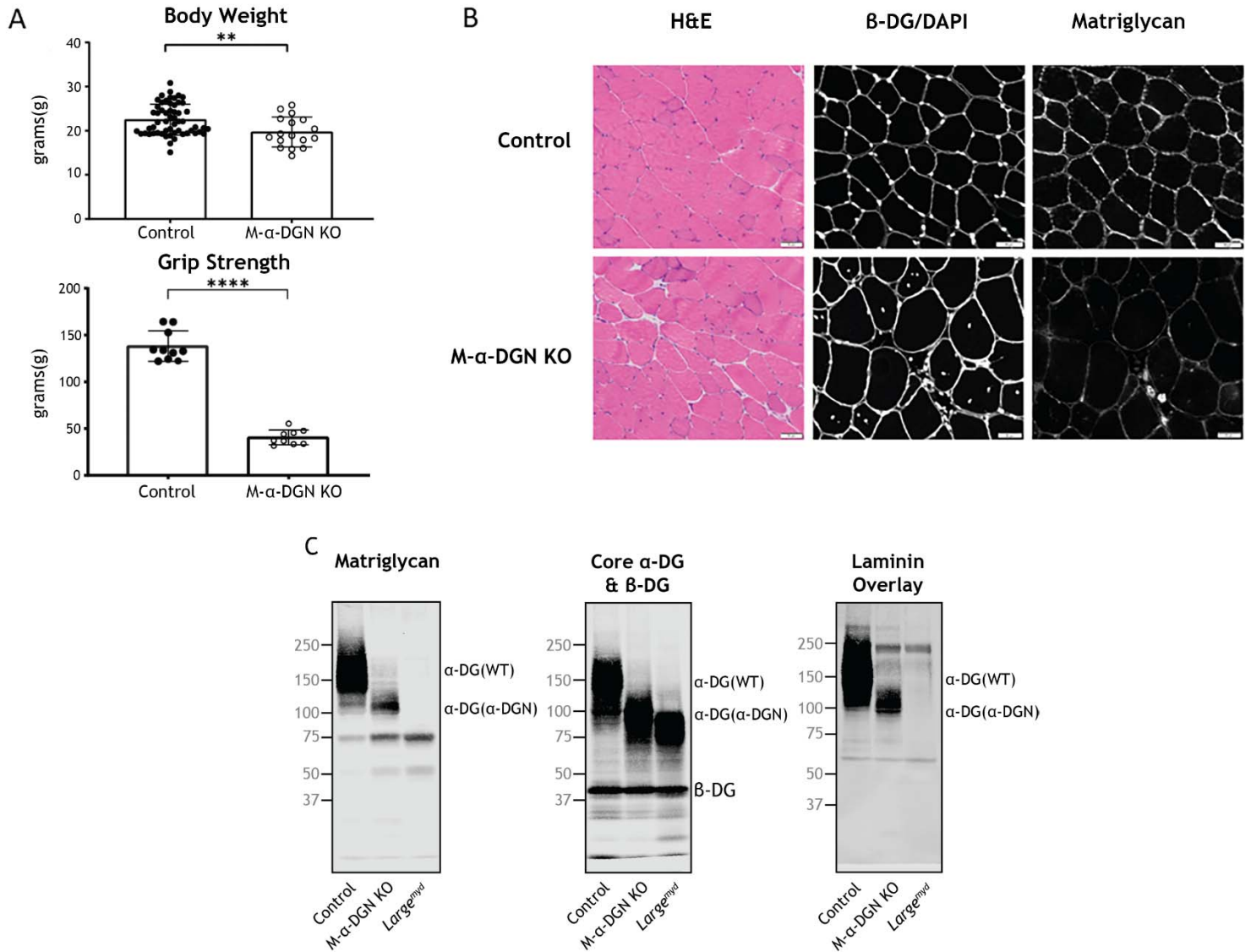
86

87 **Figure 1. Domain structure of DG and $\Delta\text{-}\alpha\text{-DG}$.** Wild-type DG is a pre-proprotein with an
88 N-terminal signal peptide (light green) that is translated in the rough endoplasmic reticulum. The
89 globular N-terminal domain ($\alpha\text{-DGN}$; orange) is present in wild-type DG but absent in the
90 mutant ($\Delta\text{-}\alpha\text{-DG}$). The junction between $\alpha\text{-DGN}$ and the mucin-like domain (light teal)
91 contains a furin convertase site. The globular extracellular C-terminal domain (CTD; pink)
92 contains a SEA (sea urchin sperm protein, enterokinase and agrin) autoproteolysis site, which
93 cleaves pro-DG into $\alpha\text{-DG}$ and $\beta\text{-DG}$ (green). Glycosylation has been omitted for clarity.

94 **Results**

95 To ablate α -DGN in skeletal muscle, we used mice expressing Cre recombinase under the
96 control of the *paired box 7 (Pax7)* promoter ($Pax7^{Cre}$), floxed DG mice ($Dag1^{lox/lox}$), and
97 heterozygous α -DGN deleted mice ($Dag1^{wt/\Delta\alpha-DGN}$) to generate $Pax7^{Cre} Dag1^{lox/\Delta\alpha-DGN}$ (M- α -DGN
98 KO) mice (**Figure 2**). Constitutive deletion of DG in mice causes embryonic lethality due to the
99 absence of Reichert's membrane, an extraembryonic basement membrane required for *in utero*
100 development (*Williamson et al., 1997*). Deletion of α -DGN in mice also causes embryonic
101 lethality (*de Greef et al., 2019*). However, mice that are heterozygous for α -DGN deletion are
102 viable and express α -DG of two different sizes (**Figure 2-figure supplement 1**) corresponding to
103 both wild-type (WT) and the α -DGN-deleted ($\Delta\alpha$ -DGN) forms of DG.

104 To evaluate the gross phenotype of mice expressing only α -DGN-deleted DG in skeletal
105 muscle (i.e., M- α -DGN KO mice), we first measured body weight and grip strength. M- α -DGN
106 KO mice were lower in weight than WT littermates (control) mice at 12 weeks and they
107 exhibited decreased forelimb grip strength (**Figure 2A**). To determine whether deletion of α -
108 DGN affects matriglycan expression, we performed histological analysis of quadriceps muscle
109 from control or M- α -DGN KO mice. M- α -DGN KO mice showed characteristic features of
110 muscular dystrophy, including an increase in centrally nucleated fibers (**Figure 2B**).
111 Immunofluorescence analyses of M- α -DGN KO muscle showed reduced levels of matriglycan
112 relative to controls, but a similar expression of β -DG, the transmembrane subunit of DG (**Figure**
113 **2B**).

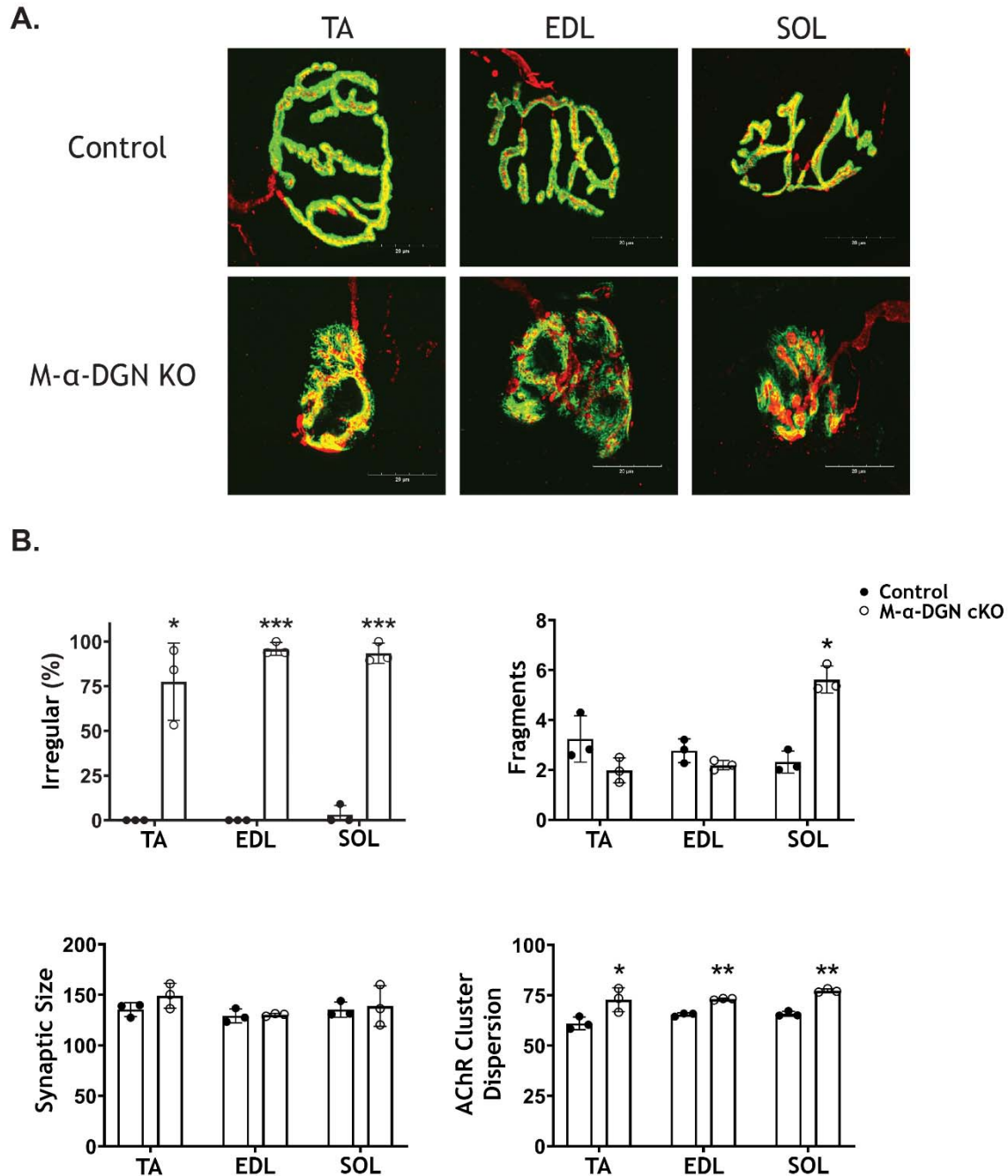


114
 115 **Figure 2. Characterization of muscle-specific α -DGN-deficient mice** (A) Body weight and
 116 grip strength of 12-week-old WT littermates (control) and M- α -DGN KO mice. Double and
 117 quadruple asterisks: statistical significance determined by Student's unpaired t-test (**p-
 118 value=0.005, ****p-value<0.0001). (B) Histological analyses of quadriceps muscles from 12-
 119 week-old control and M- α -DGN KO mice. Sections stained with H&E or used for
 120 immunofluorescence to detect β -DG (affinity purified rabbit anti- β -DG), DAPI, and matriglycan
 121 (IIIH6). (C) Immunoblot analysis of quadriceps skeletal muscle from control, M- α -DGN KO, and
 122 *myd* mice. Glycoproteins were enriched using wheat-germ agglutinin (WGA)-agarose with 10
 123 mM EDTA. Immunoblotting was performed to detect matriglycan (IIIH11), core α -DG, β -DG
 124 (AF6868), and laminin overlay. α -DG in WT control muscle (α -DG (WT)) and α -DG in α -DGN-
 125 deficient muscle (α -DG ($\Delta\alpha$ -DGN)) are indicated on the right. Molecular weight standards in
 126 kilodaltons (kDa) are shown on the left.

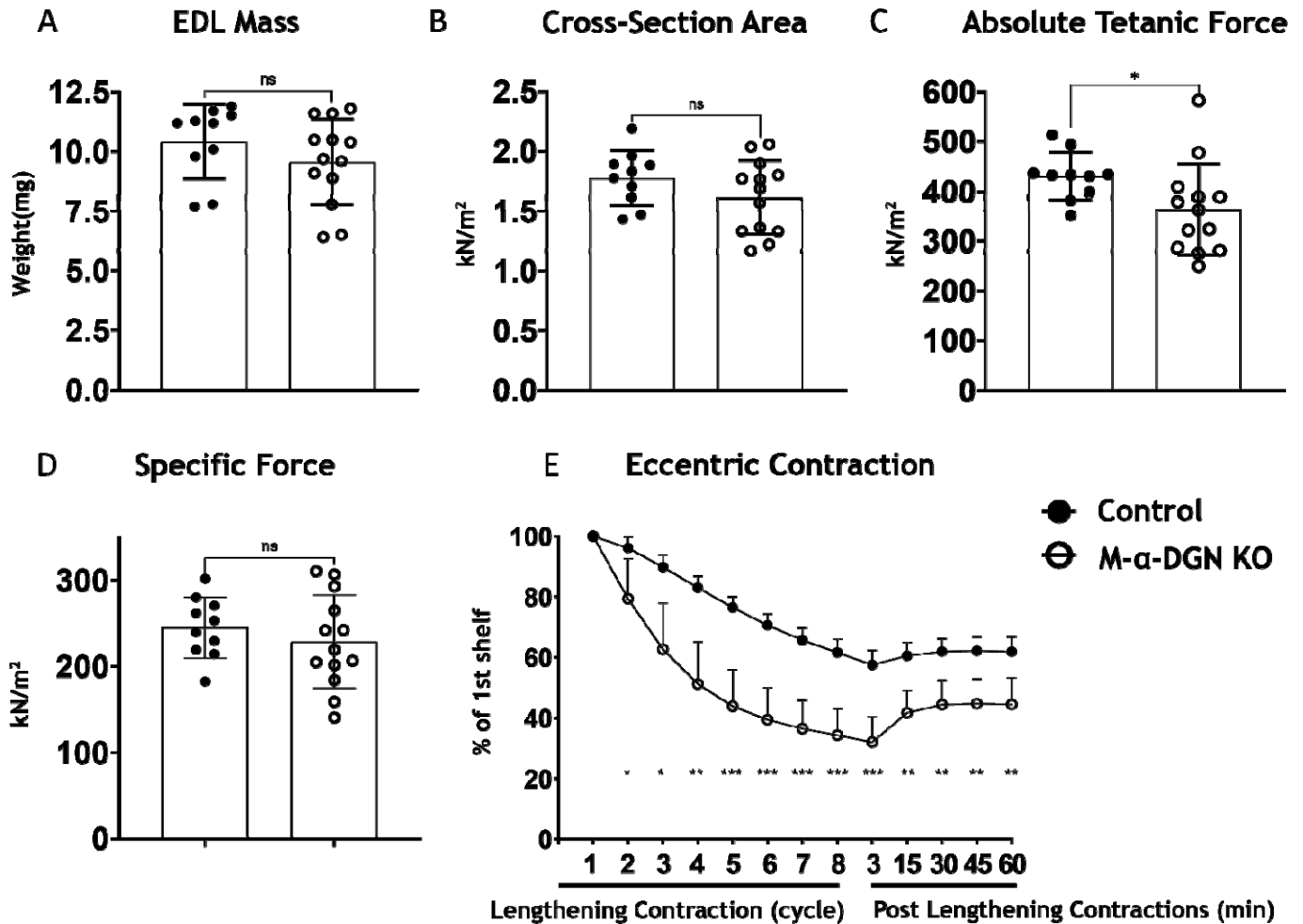
127 Immunoblot analysis of skeletal muscle from M- α -DGN KO mice demonstrated
128 expression of a shorter form of matriglycan resulting in a ~100-125 kDa α -DG, a decrease in the
129 molecular weight of the core α -DG, and no change in β -DG (**Figure 2C**). No matriglycan is seen
130 in *myd* mice which have a deletion in *Large1* (**Figure 2C**). To investigate how the loss of α -
131 DGN affected ligand binding, we performed a laminin overlay using laminin-111. Skeletal
132 muscle from control mice showed a broad band centered at ~100-250 kDa, indicative of α -DG-
133 laminin-binding; in contrast, we observed laminin-binding at ~100-125 kDa in M- α -DGN KO
134 skeletal muscle (**Figure 2c**). To further confirm that the ~100-125 kDa band seen with anti-
135 matriglycan antibodies in M- α -DGN KO muscle is matriglycan, we digested it overnight with β -
136 glucuronidase (*Thermotoga maritima*) and α -xylosidase (*Sulfolobus solfataricus*). Immunoblot
137 analysis after digestion with anti-matriglycan antibodies or laminin overlay revealed that the
138 ~100-125 kDa was completely lost, indicating that the ~100-125 kDa band is indeed matriglycan
139 on α -DG (**Figure 2-figure supplement 2**).

140 The neuromuscular junctions (NMJs) in adult control mice showed a normal pretzel-like
141 shape whereas NMJs from M- α -DGN KO mice displayed a variety of abnormalities, including a
142 granular appearance and AChR-rich streaks extending beyond the pre-synaptic terminal (**Figure**
143 **3**). Postsynaptic morphology in adult M- α -DGN KO mice was predominately irregular in the
144 tibialis anterior (TA), extensor digitorum longus (EDL), and soleus (SOL) muscles (**Figure 3**).
145 Although the overall synaptic size did not differ between controls and M- α -DGN KO mice, the
146 dispersion of AChR clusters was greater in the M- α -DGN KOs (**Figure 3**), in line with an
147 increased percentage of plaque-like formations and AChR extensions that projected beyond the
148 nerve terminal. Despite the post-synaptic abnormalities, all NMJs from M- α -DGN KO mice
149 were fully innervated.

150 To determine the effect that the loss of α -DGN has on muscle force production, we
151 characterized the phenotype and function of extensor digitorum longus (EDL) muscles in 12-17-
152 week-old WT (control) and M- α -DGN KO mice. Specifically, we measured muscle mass,
153 muscle cross-sectional area (CSA), production of absolute isometric tetanic force, specific force,
154 and lengthening contraction-induced reduction in force. Muscle mass and CSA were comparable
155 between control and M- α -DGN KO mice (**Figure 4A and B**). Although the production of
156 absolute isometric tetanic force was significantly lower in M- α -DGN KO mice than in control
157 mice (**Figure 4C**), specific forces were comparable between the two groups when normalized to
158 muscle CSA (**Figure 4D**). Lengthening contraction-induced reduction in force for M- α -DGN
159 KO EDL remained greater than those from control EDL for the entire 60 minutes that muscles
160 were assessed (**Figure 4E**). These results suggest that the short form of matriglycan on α -DG in
161 M- α -DGN KO mice enables force production but cannot prevent force reduction caused by
162 lengthening contractions. POMK KO skeletal muscle also expresses a short form of matriglycan,
163 similar to M- α -DGN KO muscle, which maintains force production but cannot prevent
164 lengthening contraction-induced force decline (**Walimbe et al., 2020**). Therefore, we compared
165 the muscle function of EDL muscles from POMK KO mice with those from M- α -DGN KO *ex*
166 *vivo*. We did not observe significant differences in lengthening contraction-induced force deficits
167 between the two mouse strains (**Figure 4-figure supplement 1**). These results suggest that
168 matriglycan of a similar molecular weight exhibits similar muscle force production and
169 lengthening contraction-induced force decline.



170
171 **Figure 3. α -DGN deficiency results in postsynaptic defects.** Neuromuscular junctions (NMJs)
172 from tibialis anterior (TA), extensor digitorum longus (EDL), and soleus (SOL) muscles
173 obtained from 35-39-week-old adult control and M- α -DGN KO mice. (A) Representative images
174 of post-synaptic terminals (α -BTX-488; green), motor axons (anti-neurofilament-H; red), and
175 pre-synaptic terminals (anti-synaptophysin; red) from TA, EDL, and SOL muscles. Scale bars =
176 20 μ m. (B) Scoring of postsynaptic defects by blinded observers (scoring criteria described in
177 Methods). Statistical significance determined by Student's unpaired t-test; * p-value < 0.05; **
178 p-value < 0.001; *** p-value < 0.0001.



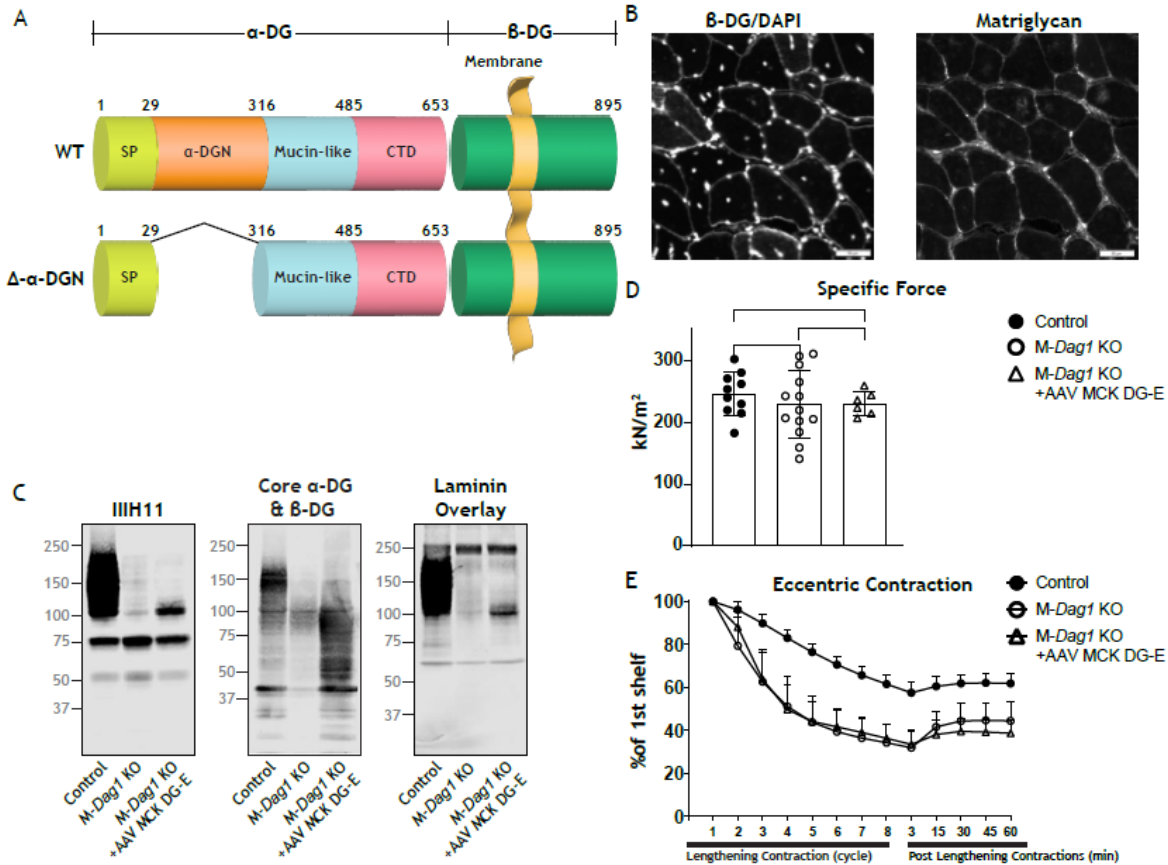
179

180 **Figure 4. α -DGN-deficient Extensor Digitorum Longus (EDL) muscle demonstrates a**
 181 **decline in lengthening contraction-induced force.** (A) Weight (milligrams) of EDL muscles
 182 from WT littermates (controls) and M- α -DGN KO mice; $p=0.2469$, as determined by Student's
 183 unpaired t-test. (B) Cross-sectional area of EDL muscles; $p=0.1810$, as determined by Student's
 184 unpaired t-test. (C) Maximum absolute tetanic force production in EDL muscles. $p=0.0488$, as
 185 determined by Student's unpaired t-test. (D) Specific Force production in EDL muscles;
 186 $p=0.4158$, as determined by Student's unpaired t-test. (E) Force deficit and force recovery after
 187 eccentric contractions in EDL muscles from 12- to 17-week-old male & female control (closed
 188 circles; $n=7$) and M- α -DGN KO (open circles; $n=7$) mice. * $p<0.05$; ** $p<0.01$; *** $p<0.001$, as
 189 determined by Student's unpaired t-test of at any given lengthening contractions cycle. Bars
 190 represent the mean +/- the standard deviation.

191 We next determined if exogenous DG lacking α -DGN (**Figure 5**) produces the short form
192 of matriglycan. We first produced muscle-specific DG KO mice to achieve muscle-specific
193 deletion of DG. To do this, we used mice expressing Cre under control of the paired box 7
194 (Pax7) promoter (Pax7-Cre) and *Dag1*^{flox/flox} mice to generate Pax7Cre; *Dag1*^{flox/flox} (M-*Dag1*
195 KO) mice. To assess muscle function, we evaluated muscle-specific force and lengthening
196 contraction-induced reduction in force *ex vivo*, which showed that muscle-specific force was
197 significantly decreased and that muscles were more susceptible to lengthening contraction-
198 induced force decline in the absence of DG (**Figure 5-figure supplement 1**). Collectively, these
199 results show that M-*Dag1* KO mice harbor a more complete deletion of DG in muscle than the
200 previously generated mouse model (MCK-Cre *Dag1*^{flox/flox}) harboring muscle-specific deletion of
201 DG (**Cohn et al., 2002**). To assess the presence of DG, we performed immunostaining of
202 quadriceps muscles from 12-week-old M-*Dag1* KO mice, which showed the absence of DG-
203 positive fibers (**Figure 5-figure supplement 1**). Immunoblot analysis showed that matriglycan
204 and α -DG derived from skeletal muscle were not observed in M-*Dag1* KO mice (**Figure 5-
205 figure supplement 1**). This is consistent with prior reports showing that only peripheral-nerve
206 derived matriglycan of 110 kDa is observed in M-*Dag1* KO mice in the presence of EDTA,
207 which improves the extraction of matriglycan positive α -DG and acts as a protease inhibitor by
208 chelating calcium (**Saito et al., 2003**).

209 We next generated an adeno-associated virus (AAV) construct of DG lacking the α -DGN
210 (AAV-MCK DG-E; **Figure 5A**), which we injected into M-*Dag1* KO mice through the retro-
211 orbital sinus. A previous report found that matriglycan was not produced when a similar
212 adenovirus construct of DG lacking the α -DGN was used to infect ES cells (**Kanagawa et al.,
213 2004**). However, we found that matriglycan of similar size was produced in M-*Dag1* KO mice

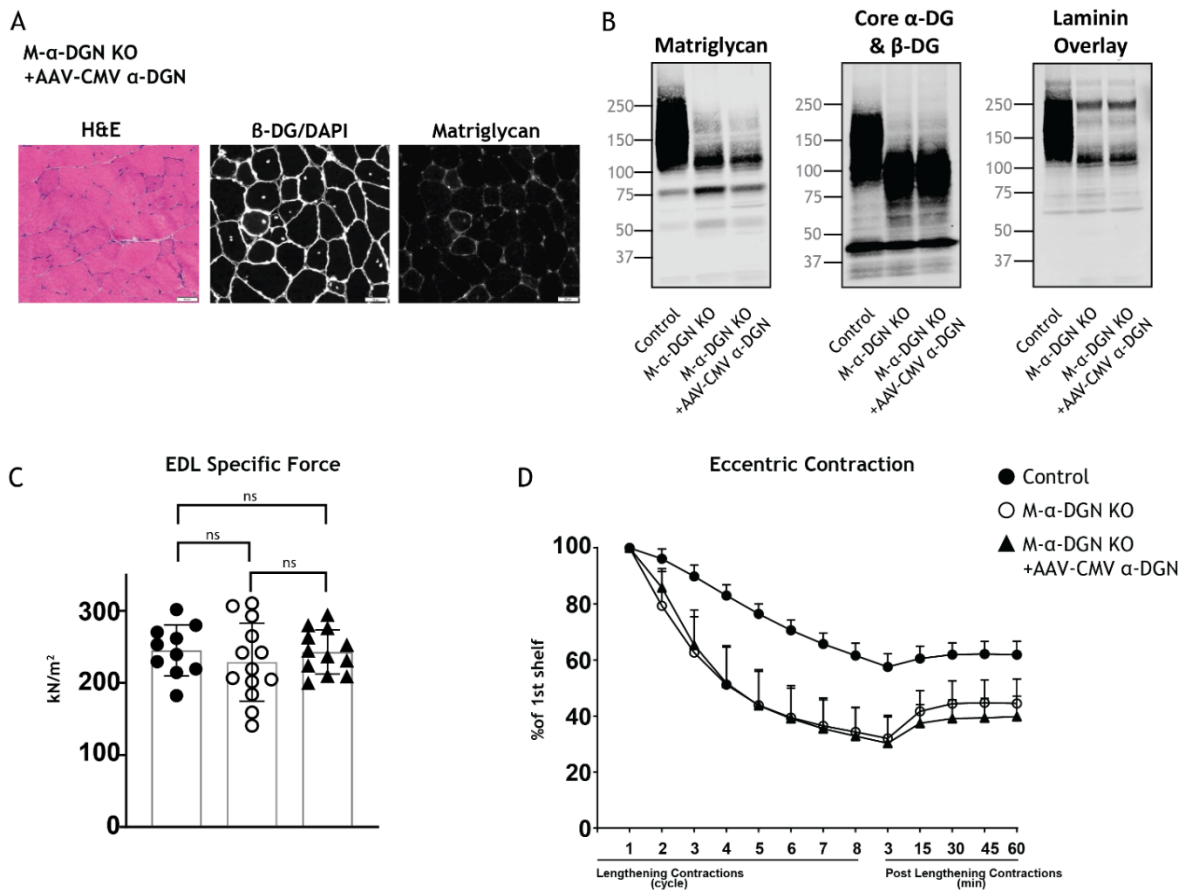
214 injected with AAV-MCK DG-E as in M- α -DGN KO mice (**Figure 5**). Immunofluorescence
215 analysis of quadriceps muscle from M-*Dag1* KO mice injected with AAV-MCK DG-E showed
216 decreased immunoreactivity to matriglycan-positive muscle fibers but restored expression of β -
217 DG (**Figure 5B**). Immunoblot analysis of skeletal muscle from M-*Dag1* KO mice injected with
218 AAV-MCK-DG-E showed expression of α -DG containing matriglycan around ~100-125 kDa
219 (**Figure 5C**), which was the same size as α -DG with matriglycan in M- α -DGN KO (**Figure 2C**).
220 The molecular weight of α -DG was decreased in muscle from these mice, similar to that
221 observed in M- α -DGN KO mice, whereas the molecular weight of β -DG was unchanged relative
222 to M- α -DGN KO mice (**Figure 2C**). We also observed laminin-binding at ~100-125 kDa in
223 muscle from M-*Dag1* KO + AAV-MCK DG-E mice (**Figure 5C**). In addition, we assessed the
224 physiologic effects of expressing DG without the N-terminal domain. We observed that the
225 specific force was comparable in M-*Dag1* KO + AAV-MCK DG-E and M- α -DGN KO mice
226 (**Figure 5D**) and that the two groups exhibited similar amounts of lengthening contraction-
227 induced force decline (**Figure 5E**). Therefore, these data demonstrate that AAV-mediated
228 delivery of exogenous DG lacking the α -DGN into an M-*Dag1* KO mouse also produces short
229 matriglycan and exhibits the same muscle function as M- α -DGN KO mice.



230
 231 **Figure 5. Exogenous α -DGN-deficient DG also produces short matriglycans similar to M-**
 232 ***Dag1* KO mice. (A)** Schematic representation of WT DG, adeno-associated virus (AAV), and a
 233 mutant DG in which the N-terminal domain has been deleted (DG-E) adeno-associated virus. α -
 234 DG is composed of a signal peptide (SP, amino acids 1–29), an N-terminal domain (amino acids
 235 30–316), a mucin-like domain (amino acids 317–485), and a C-terminal domain (amino acids
 236 486–653). The green box represents β -DG. **(B)** Immunofluorescence analyses of quadriceps
 237 muscles from 12-week-old *M-Dag1* KO mice injected with AAV-MCK DG-E to detect β -DG,
 238 nuclei (DAPI) and matriglycan (IIIH6). **(C)** Immunoblot analysis of skeletal muscle obtained
 239 from littermate controls (control), *M-Dag1* KO mice or *M-Dag1* KO mice injected with AAV-
 240 MCK DG-E. Glycoproteins were enriched from quadriceps skeletal muscles using WGA-agarose
 241 with 10 mM EDTA. Immunoblotting was performed to detect matriglycan (IIIH11), core α -DG
 242 and β -DG (AF6868), and laminin (overlay). **(D)** Production of specific force in EDL muscles
 243 from 12- to 17-week-old male & female *M-Dag1* KO mice (controls; closed circles, n=10); M-
 244 α -DGN KO mice (open circles, n=13); and *M-Dag1* KO+AAVMCK DG-E mice (open triangles,
 245 n=6). P-values determined by Student's unpaired t-test; controls vs *M-Dag1* KO: p=0.4158;
 246 controls vs *M-Dag1* KO+AAVMCK DG-E: p=0.3632; *M-Dag1* KO vs *M-Dag1* KO+AAVMCK
 247 DG-E: p=0.948. **(E)** Force deficits and recovery in EDL muscles from mice in D. There is no
 248 significant difference in *M-Dag1* KO vs *M-Dag1* KO+AAVMCK DG-E as determined by
 249 Student's unpaired t-test at any given lengthening contraction cycle or post-lengthening
 250 contraction.

251 Our studies show that DG lacking the α -DGN expresses a short form of matriglycan; this
252 suggests that α -DGN is necessary for the production of full-length matriglycan. To test this
253 hypothesis, we determined if matriglycan expression could be restored in mice lacking α -DGN.
254 We injected M- α -DGN KO mice with an AAV expressing α -DGN (AAV-CMV α -DGN) and
255 harvested the skeletal muscles of these mice eight to ten weeks after injection. H&E staining in
256 M- α -DGN KO mice injected with AAV-CMV α -DGN was unchanged from M- α -DGN KO mice
257 (**Figure 2B, 6A**). Quadriceps muscles from M- α -DGN KO mice injected with AAV-CMV α -
258 DGN showed a reduced intensity of matriglycan relative to LCs (**Figure 6A**). Immunoblot
259 analysis of these mice showed that matriglycan had a molecular weight of ~100-125 kDa and the
260 size of α -DG was shifted down, whereas β -DG remained unchanged (**Figure 6B**). Laminin-
261 binding was observed at ~100-125 kDa in M- α -DGN KO skeletal muscle infected with AAV-
262 CMV α -DGN (**Figure 6B**). Collectively, this phenotype is similar to that observed in the skeletal
263 muscles of M- α -DGN KO mice. Expressing α -DGN in M- α -DGN KO mice did not alter specific
264 force or improve force deficits induced by lengthening contractions (**Figure 6C, 6D**). Thus,
265 supplementing M- α -DGN KO skeletal muscle with α -DGN fails to improve matriglycan
266 elongation.

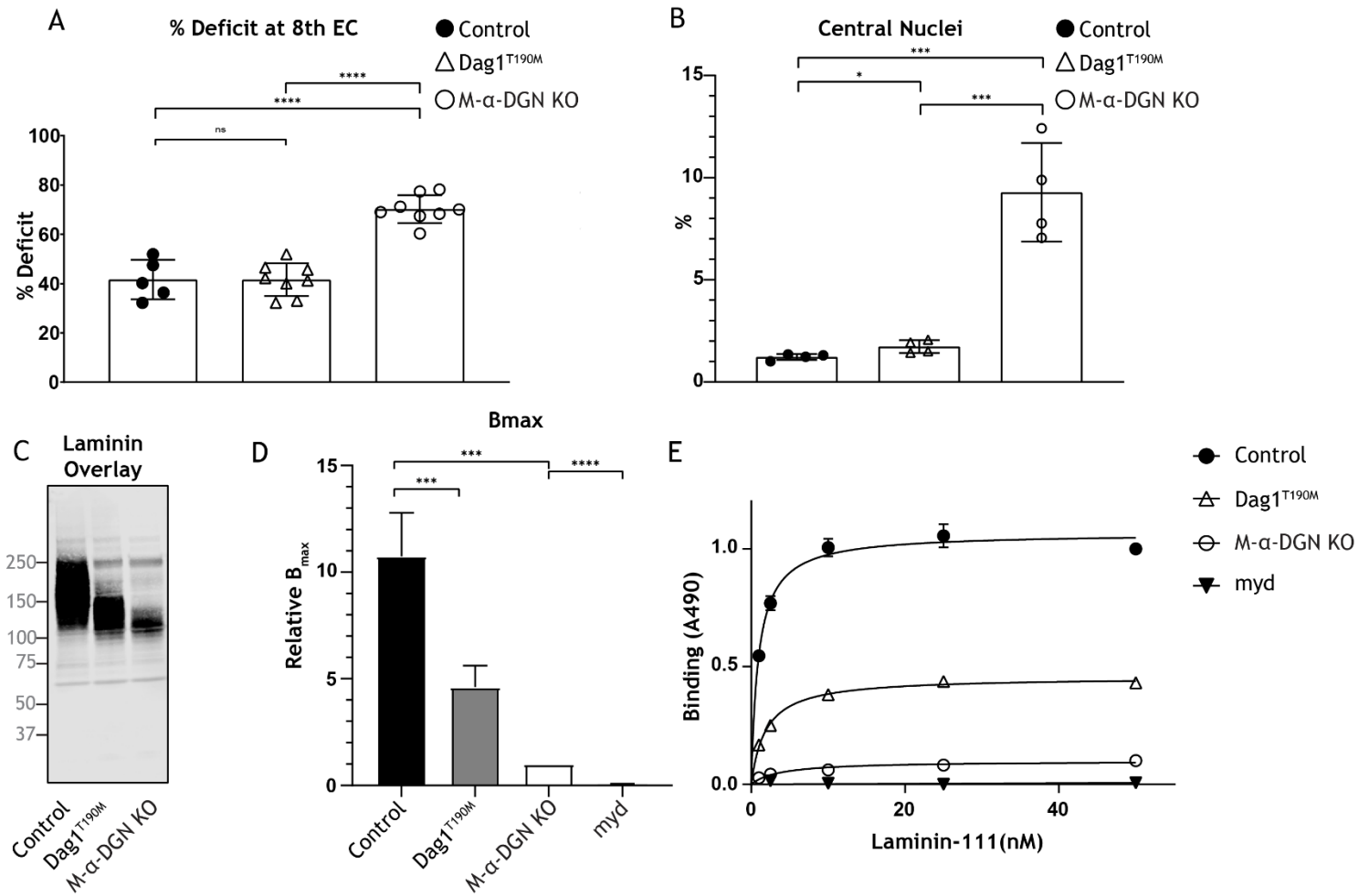
267 To determine if excess LARGE1 produces full-size matriglycan in M- α -DGN KO
268 muscle, we evaluated immunoblot analysis of skeletal muscle from LCs, M- α -DGN KO, and M-
269 α -DGN KO mice injected with AAV-MCK-Large1. M- α -DGN KO mice injected with AAV-
270 MCK-Large1 demonstrated no change in the molecular weight of matriglycan, α -DG, and β -DG
271 relative to M- α -DGN KO. A laminin overlay using laminin-111 also showed no change (**Figure**
272 **6-figure supplement 1**). These results indicate that even if LARGE1 is overexpressed, full-size
273 matriglycan cannot be produced without α -DGN.



274
275 **Figure 6. Expression of α -DGN in M- α -DGN KO mice does not rescue matriglycan**
276 **elongation.** (A) Representative sections of quadriceps muscles from 17-week-old M- α -DGN KO
277 mice injected with AAV-CMV α -DGN. Sections were stained with H&E and
278 immunofluorescence to detect matriglycan (IIIH6) and β -DG (AP83). (B) Immunoblot analysis of
279 skeletal muscle obtained from littermate controls or M- α -DGN KO mice and M- α -DGN KO
280 mice injected with AAV-CMV α -DGN (M- α -DGN KO+AAV-CMV α -DGN). Glycoproteins
281 were enriched using WGA-agarose with 10 mM EDTA. Immunoblotting was performed to
282 detect matriglycan (IIIH11), core α -DG and β -DG (AF6868), and laminin overlay. (C)
283 Production of specific force in EDL muscles from 12- to 17-week-old male & female M- α -DGN
284 WT littermates (controls; closed circles, n=10); M- α -DGN KO (open circles, n=13); and M- α -
285 DGN KO+AAV-CMV α -DGN (closed triangles, n=12). P-values determined by Student's
286 unpaired t-test; controls vs M- α -DGN KO+AAV-CMV α -DGN: p=0.8759; controls vs M- α -
287 DGN KO: p=0.4333; M- α -DGN KO vs M- α -DGN KO+AAV-CMV α -DGN: p=0.4333. (D)
288 Force deficit and force recovery after lengthening contractions in EDL muscles from 12- to 17-
289 week-old male & female M- α -DGN KO WT littermates (controls, closed circles; n=6) and M- α -
290 DGN KO (KO, open circles; n=7) mice, and in M- α -DGN KO mice injected with AAV-CMV α -
291 DGN (KO+AAV-CMV α -DGN, closed triangles; n=8). There is no significant difference in M-
292 α -DGN KO vs M- α -DGN KO+AAV-CMV α -DGN as determined by Student's unpaired t-test at
293 any given lengthening contractions cycle or post lengthening contractions.

294 The length of matriglycan is correlated with its ability to bind ECM ligands (*Goddeeris et*
295 *al., 2013*). Therefore, we hypothesized that the susceptibility to force decline by lengthening
296 contractions would differ depending on the length of matriglycan. To test this, we performed
297 physiological muscle tests in three different mouse models to determine the difference in
298 susceptibility to lengthening contraction-induced reduction in force. Specifically, we used: 1) M-
299 α -DGN KO mice, which express a short form of matriglycan, 2) *Dagl*^{T190M} mice, which harbor a
300 knock-in mutation (T190M) in *DAG1* that inhibits the DG-LARGE1 interaction and leads to
301 incomplete post-translational modification of α -DG (*Hara et al., 2011*), and 3) C57BL/6J WT
302 (C57) mice, which have full-length matriglycan. The percent deficit value of the 8th eccentric
303 contraction (EC) shows the largest difference in the EC protocol; therefore, we compared these
304 values between our three different mouse models (*Figure 7A*). M- α -DGN KO mice showed a
305 significantly higher percent deficit ($70.2\% \pm 5.7$) compared to C57 ($41.7\% \pm 8.0$) and *Dagl*^{T190M}
306 (41.6 ± 6.7) mice, with no difference observed between the latter groups. Immunoblot analysis of
307 laminin in skeletal muscle showed α -DG laminin-binding at ~150-250 kDa in skeletal muscle
308 from C57 mice, ~100-150 kDa in skeletal muscle from *Dagl*^{T190M} mice, and ~100-125 kDa in
309 skeletal muscle from M- α -DGN KO mice (*Figure 7C*). Moreover, the percentage of centrally
310 nucleated fibers differed significantly in *Dagl*^{T190M} ($1.73\% \pm 0.31$) and M- α -DGN KO
311 ($9.28\% \pm 2.41$) mice compared to C57 mice ($1.22\% \pm 0.15$) (*Figure 7B*). The reduction of laminin-
312 binding activity of α -DG is thought to be the main cause of dystroglycanopathy (*Kanagawa et*
313 *al., 2009; Goddeeris et al., 2013*). Indeed, we observed a reduced binding capacity (relative
314 B_{\max}) for laminin-111 in solid-phase binding analyses in skeletal muscle from M- α -DGN KO and
315 *Dagl*^{T190M} mice compared to skeletal muscle from C57 mice (10.7-fold and 2.3-fold difference
316 relative to WT, respectively) (*Figure 7D*). However, the binding capacity of skeletal muscle

317 from *Dagl*^{T190M} and M- α -DGN KO mice was higher than that of *myd* muscle (**Figure 7E**). M- α -
318 DGN KO and *Dagl*^{T190M} also displayed an increase in dissociation constant (**Figure 7E**).
319 Collectively, these results suggest that α -DG positive matriglycan of at least ~150 kDa is
320 sufficient to prevent force decline from lengthening contractions and significant dystrophic
321 changes, despite a 45% reduction in laminin-binding activity.



322 **Figure 7. Relationship between matriglycan length and dystrophic phenotype.** (A) % deficit
 323 of 8th eccentric contraction (EC) in EDL muscles from C57BL/6J WT (control), M-α-DGN KO,
 324 and *Dag1*^{T190M} mice. p-values determined by Student's unpaired t-test; control vs *Dag1*^{T190M}:
 325 p=0.0263; control and *Dag1*^{T190M} vs M-α-DGN KO: p<0.001. (B) Percentage of muscle fibers
 326 with central nuclei in 12- to 19-week-old control, *Dag1*^{T190M} and M-α-DGN KO mice; n=4 for all
 327 groups. P-values determined by Student's unpaired t-test; control and *Dag1*^{T190M} vs M-α-DGN
 328 KO: p<0.001; control vs *Dag1*^{T190M}: p=0.0263. (C) Immunoblot analysis of quadriceps skeletal
 329 muscles from control, *Dag1*^{T190M} and M-α-DGN KO mice. Glycoproteins were enriched using
 330 WGA-agarose with 10 mM EDTA. Immunoblotting was performed with laminin (laminin
 331 overlay). (D) Comparison of average solid-phase determined relative B_{max} values for laminin.
 332 B_{max} values for M-α-DGN KO were set to 1 to allow for direct comparisons; error bars indicate
 333 s.e.m. P-values determined using Student's unpaired t-test; control vs *Dag1*^{T190M} and control vs
 334 M-α-DGN KO: p<0.01, and M-α-DGN KO vs *myd*: p<0.001. (E) Solid-phase analysis of
 335 laminin-binding using Laminin-111 in skeletal muscle from control, *Dag1*^{T190M}, M-α-DGN KO,
 336 and *myd* KO mice (three replicates for each group). Control K_d: 0.9664 ± 0.06897 nM;
 337 *Dag1*^{T190M} K_d: 1.902 ± 0.1994 nM; and M-α-DGN KO K_d: 2.322 ± 0.6114 nM.

338 **Discussion**

339 Functional glycosylation of α -DG requires α -DGN (*Kanagawa et al., 2004; Hara,*
340 *Kanagawa, et al., 2011*). However, it remains unclear how the loss of α -DGN affects
341 matriglycan synthesis. Here, we show that the lack of α -DGN does not preclude matriglycan
342 synthesis entirely. Instead, in the absence of α -DGN, LARGE1 synthesizes a short, non-
343 elongated form of matriglycan on α -DG (~100-125 kDa), which demonstrates that the N-
344 terminal domain is required for matriglycan elongation. Thus, LARGE1- α DGN holds the
345 enzyme-substrate complex together over multiple cycles of sugar addition. These findings build
346 on our previous study demonstrating that phosphorylation of the core M3 trisaccharide by
347 POMK is also necessary for matriglycan elongation (*Walimbe et al., 2020*). Thus, the generation
348 of full-length mature matriglycan on α -DG (~150-250 kDa) by *LARGE1* requires both POMK
349 and α -DGN to be bound to DG; in the absence of either, a shorter form is generated.

350 In our study, muscle-specific deletion of α -DGN resulted in the production of short forms
351 of matriglycan on α -DG (~100-125 kDa). Mice lacking α -DGN exhibited low bodyweight and
352 grip strength, and histological characterization of quadriceps muscles revealed mild muscular
353 dystrophy and a lack of homogeneous matriglycan expression. Physiological examination
354 revealed that M- α -DGN KO muscle was susceptible to lengthening contraction-induced force
355 decline, although specific force was maintained. These results are consistent with those obtained
356 when α -DGN-deleted DG was administered to muscle-specific DG KO mice and indicates that
357 DG lacking α -DGN produces short forms of matriglycan, which does not prevent dystrophic
358 muscle changes in this mouse model. Furthermore, DG in the postsynaptic membrane is known
359 to play a key role in synaptic maturation (*Nishimune et al., 2008*). However, the NMJs in M- α -

360 DGN KO mice in our study were abnormal and irregularly shaped. This indicates both that DG
361 and matriglycan are required for synaptic maturation.

362 If LARGE1 binding to α -DGN enables its ability to elongate matriglycan, then we would
363 expect that rescuing M- α -DGN KO skeletal muscle with α -DGN would restore the expression of
364 full-length matriglycan. However, this failed to occur and indicates that solely restoring α -DGN
365 expression is not sufficient for LARGE1 to elongate matriglycan. These results indicate that the
366 ability for LARGE1 to elongate matriglycan requires α -DGN to be attached to DG. This finding
367 is consistent with data showing that matriglycan is not elongated when α -DGN is deleted, even
368 when LARGE1 is overexpressed. Therefore, α -DGN acts as a recognition site for the
369 glycosyltransferase *LARGE1* and establishes a model where α -DGN, together with
370 phosphorylated core M3, anchors *LARGE1* to the matriglycan production site to enable its
371 synthesis and elongation. Notably, although the molecular recognition of α -DGN by *LARGE1* is
372 considered essential for the expression of functional DG (*Kanagawa et al., 2004*), our results
373 show that *LARGE1* can synthesize a short non-elongated form of matriglycan in the absence of
374 α -DGN, indicating that LARGE1 is capable of adding matriglycan to α -DG independent of its
375 interaction with α -DGN.

376 To determine how much matriglycan is needed to prevent lengthening contraction-
377 induced reduction in force, we used mice that express different sizes of matriglycan. Muscle
378 from M- α -DGN KO mice showed an increased force deficit and a 7.6-fold increase in centrally
379 nucleated fibers compared to muscle from C57 mice, indicating that short forms of matriglycan
380 do not prevent dystrophic changes. However, despite the lower amount of matriglycan in muscle
381 from *Dagl^{T190M}* mice compared to that from C57 mice, the force deficit was not different
382 between the two groups, and centrally nucleated fibers were increased in α -DGN mutant

383 (T190M) mice by only 1.4-fold. This indicates that short matriglycan, if over 150kDa, can
384 prevent muscular dystrophy.

385 Muscular dystrophy is not observed in a mouse model of Fukuyama congenital muscular
386 dystrophy, which occurs due to a retrotransposition insertion in the mouse *fukutin* ortholog and
387 causes laminin-binding at 50% of normal levels (*Kanagawa et al., 2009*). In *Dagl*^{T190M} mice, the
388 laminin-binding level is about 45% of normal, which likely explains a mild increase in centrally
389 nucleated fibers compared to C57 muscle. However, in muscle from M- α -DGN KO mice, the
390 laminin-binding level is only 9% relative to that of C57 mice and leads to a marked increase in
391 centrally nucleated fibers and force deficit induced by lengthening contractions. This indicates
392 that matriglycan length is critical for regulating damage induced by lengthening contractions and
393 that the production of ~120-150 kDa α -DG significantly prevents dystrophic change, suggesting
394 that this pathologic effect can be prevented without the expression of full-length matriglycan.
395 Thus, our results describe a relationship between matriglycan size, damage induced by
396 lengthening contractions, and the degree of dystrophic change. However, the difference between
397 the abundance of central nuclei and the results of damage due to lengthening contractions in C57
398 and *Dagl* mice indicate that other factors likely contribute to normal physiologic function in
399 muscle.

400 Collectively our study demonstrates that α -DG with α -DGN is required for the synthesis
401 of full-length matriglycan on α -DG (~150-250 kDa). In the absence of α -DGN, LARGE1 can
402 synthesize a short non-elongated form of matriglycan on α -DG (~100-125kDa) in skeletal
403 muscle in a process that is independent of its interaction with α -DGN. These findings are
404 essential for a complete understanding of the mechanisms underlying matriglycan synthesis and

405 show that matriglycan length regulates the severity of muscular dystrophy and may serve as a
406 therapeutic target for the treatment of α -dystroglycanopathy.

407 **Materials and methods**

408 **Animals**

409 All mice were maintained in a barrier-free, specific pathogen-free grade facility and had access
410 to normal chow and water *ad libitum*. All animals were manipulated in biosafety cabinets and
411 change stations using aseptic procedures. The mice were maintained in a climate-controlled
412 environment at 25°C on a 12/12 hour light/dark cycle. Animal care, ethical usage, and
413 procedures were approved and performed in accordance with the standards set forth by the
414 National Institutes of Health and the University of Iowa Animal Care and Use Committee
415 (IACUC). Mouse lines used in the study that have been previously described are: *Dag1*^{-/-} (JAX#
416 006836; *Williamson et al., 1997*), *Dag1*^{flox} (JAX# 009652; *Cohn et al., 2002*), *Dag1*^{Aa-DGN} (*de*
417 *Greef et al., 2019*), *Dag1*^{T190M} (*Hara et al., 2011*), *Large1*^{myd} (JAX# 000300) (*Lane et al., 1976*),
418 *Mck*^{cre} (JAX# 006475) (*Brüning et al., 1998*), *Pax7*^{cre} (JAX# 010530) (*Keller et al., 2004*), and
419 *Mck*^{cre} *Pax7*^{cre} *POMK*^{flox} (*Walimbe et al., 2020*).

420 **Muscle-specific DG knockout mice (*Pax7*^{cre} *Dag1*^{flox/flox})**

421 Male mice expressing the *Pax7-Cre* transgene were bred to female mice that were homozygous
422 for the floxed *Dag1* allele (*Dag1*^{flox/flox}). Male F1 progeny with the genotype *Pax7*^{Cre}; *Dag1*^{flox/+}
423 were bred to female *Dag1*^{flox/flox} mice. A *Cre* PCR genotyping protocol was used to genotype the
424 *Cre* allele using standard *Cre* primers. The primers used were Sense:
425 TGATGAGGTTTCGCAAGAACC and Antisense: CCATGAGTGAACGAACCTGG.
426 Genotyping of *Pax7*^{Cre}; *Dag1*^{flox/flox} mice was performed by Transnetyx using real-time PCR.

427 **Muscle-specific α -DGN knockout mice (M- α -DGN KO)**

428 Male mice expressing the *Pax7-Cre* transgene were bred to female mice that were heterozygous
429 for the *Dag1* ^{Δ α -DGN} allele (*Dag1*^{wt/ $\Delta\alpha$ -DGN}). Male F1 progeny with the genotype *Pax7*^{Cre};
430 *Dag1*^{wt/ $\Delta\alpha$ -DGN} were bred to female mice homozygous for the floxed *Dag1* allele (*Dag1*^{flox/flox}).
431 Genotyping of *Pax7*^{Cre}*Dag1*^{flox/ $\Delta\alpha$ -DGN} mice was performed by Transnetyx using real-time PCR.
432 For studies with M- α -DGN KO mice, three mice of each genotype (control and
433 *Pax7*^{Cre}*Dag1*^{flox/ $\Delta\alpha$ -DGN}) were used.
434 Littermate controls were employed whenever possible. The number of animals required was
435 based on previous studies (*de Greef et al., 2016; Goddeeris et al., 2013, Walimbe et al., 2020*)
436 and experience with standard deviations of the given techniques.

437 **Forelimb grip strength test**

438 Forelimb grip strength was measured at three months using previously published methods (*de*
439 *Greef et al., 2016, Walimbe, et al., 2020*). A mouse grip strength meter (Columbus Instruments,
440 Columbus, OH) was mounted horizontally, with a non-flexible grid connected to the force
441 transducer. The mouse was allowed to grasp the grid with its two front paws and then pulled
442 away from the grid by its tail until the grip was broken. This was done three times over five
443 trials, with a one-minute break between each trial. The gram force was recorded per pull, and any
444 pull where only one front limb or any hind limbs were used was discarded. If the mouse turned,
445 the pull was also discarded. After 15 pulls (five sets of three pulls), the mean of the three highest
446 pulls of the 15 was calculated and reported. Statistics were calculated using GraphPad Prism 8
447 software. Student's t-test was used (two-sided). Differences were considered significant at a p-
448 value less than 0.05. Graph images were also created using GraphPad Prism and the data in the
449 present study are shown as the means + / - SD unless otherwise indicated.

450 **Body weight measurements**

451 Mice were weighed as previously described (*de Greef et al., 2016, Walimbe et al., 2020*).
452 Weights were measured after testing grip strength using a Scout SPX222 scale (OHAUS
453 Corporation, Parsippany, NJ), and the tester was blinded to genotype. Statistics were calculated
454 using GraphPad Prism 8 software and Student's t-test was used (two-sided). Differences were
455 considered significant at a p-value less than 0.05. Graph images were also created using
456 GraphPad Prism and the data in the present study are shown as the means + / - SD unless
457 otherwise indicated.

458 **Measurement of *in vitro* muscle function**

459 To compare the contractile properties of muscles, EDL muscles were surgically removed as
460 described previously (*Rader et al., 2016; de Greef et al., 2016, Walimbe et al., 2020*). The
461 muscle was immediately placed in a bath containing a buffered physiological salt solution
462 (composition in mM: NaCl, 137; KCl, 5; CaCl₂, 2; MgSO₄, 1; NaH₂PO₄, 1; NaHCO₃, 24;
463 glucose, 11). The bath was maintained at 25°C, and the solution was bubbled with 95% O₂ and
464 5% CO₂ to stabilize pH at 7.4. The proximal tendon was clamped to a post and the distal tendon
465 was tied to a dual mode servomotor (Model 305C; Aurora Scientific, Aurora, ON, Canada).
466 Optimal current and whole muscle length (L₀) were determined by monitoring isometric twitch
467 force. Optimal frequency and maximal isometric tetanic force (F₀) were also determined. The
468 muscle was then subjected to an EC protocol consisting of eight ECs at three-minute intervals. A
469 fiber length L_{f-to-L₀} ratio of 0.45 was used to calculate L_f. Each EC consisted of an initial 100
470 millisecond isometric contraction at optimal frequency immediately followed by a stretch of L₀
471 to 30% of L_f beyond L₀ at a velocity of 1 L_f/s at optimal frequency. The muscle was then
472 passively returned to L₀ at the same velocity. At 3, 15, 30, 45, and 60 minutes after the EC

473 protocol, isometric tetanic force was measured. After the analysis of the contractile properties,
474 the muscle was weighed. The CSA of muscle was determined by dividing the muscle mass by
475 the product of L_f and the density of mammalian skeletal muscle (1.06 g/cm³). The specific force
476 was determined by dividing F_o by the CSA (kN/mm²). 18–20-week-old male mice were used,
477 and right and left EDL muscles from each mouse were employed whenever possible, with five to
478 eight muscles used for each analysis. Each data point represents an individual EDL. Statistics
479 were calculated using GraphPad Prism 8 software and Student's unpaired t-test was used (two-
480 sided). Differences were considered significant at a p-value less than 0.05.

481 **H&E and immunofluorescence analysis of skeletal muscle**

482 Histology and immunofluorescence of mouse skeletal muscle were performed as described
483 previously (*Goddeeris et al., 2013*). Mice were euthanized by cervical dislocation and directly
484 after sacrifice, quadriceps muscles were isolated, embedded in OCT compound and then snap
485 frozen in liquid nitrogen-cooled 2-methylbutane. 10 μ M sections were cut with a cryostat (Leica
486 CM3050S Research Cryostat; Amsterdam, the Netherlands) and H&E stained using conventional
487 methods. Whole digital images of H&E-stained sections were taken by a VS120-S5-FL Olympus
488 slide scanner microscope (Olympus Corporation, Tokyo, Japan). For immunofluorescence
489 analyses, a mouse monoclonal antibody to matriglycan on α -DG (IIH6, 1:100 dilution,
490 Developmental Studies Hybridoma Bank, University of Iowa; RRID:AB_2617216) was added to
491 sections overnight at 4 °C followed by Alexa Fluor-conjugated goat IgG against mouse IgM
492 (Invitrogen, Carlsbad, CA, 1:500 dilution) for 40 minutes. The sections were also stained with
493 rabbit polyclonal antibody to β -DG (AP83; 1:50 dilution) followed by Alexa Fluor-conjugated
494 488 Goat anti-rabbit IgG (1:500). Whole sections were imaged with a VS120-S5-FL Olympus
495 slide scanner microscope. Antibody IIH6 is a mouse monoclonal to matriglycan on α -DG

496 (*Ervasti and Campbell, 1991*), and AP83 is a rabbit polyclonal antibody to the C-terminus of β -
497 DG (*Ervasti and Campbell, 1991*), both of which have been described previously.

498 For histologic analysis of skeletal muscle, H&E staining on 10 μ M frozen section was
499 performed using the Leica ST5020 Multistainer workstation (Leica Biosystems, Buffalo Grove,
500 IL) according to the manufacturer's instructions. For immunofluorescence analysis, unfixed
501 frozen serial sections (7 μ M) were incubated with primary antibodies for one hour, and then with
502 the appropriate biotinylated secondary antibodies for 30 minutes followed by streptavidin
503 conjugated to Alexa Fluor 594 (ThermoFisher Scientific, UK) for 15 minutes. Primary antibodies
504 used were mouse monoclonal: α -DG I1H6 (clone I1H6C4) (*Ervasti and Campbell, 1991*), β -DG
505 (Leica, Milton Keynes, UK; clone 43DAG1/8D5). All washes were made in PBS and
506 incubations were performed at room temperature. Sections were evaluated with a Leica DMR
507 microscope interfaced to MetaMorph (Molecular Devices, Sunnyvale, CA).

508 **Neuromuscular Junction (NMJ) Morphology**

509 Immediately upon harvest, EDL muscles were washed in PBS three times for five minutes each.
510 EDL muscles were fixed in 4% paraformaldehyde for 20 minutes followed by three washes in
511 PBS. Fixed muscle samples were split into three to four fiber bundles before incubating in 3%
512 Triton-X 100/PBS for three hours at 4 °C. Muscles were subsequently washed in PBS followed
513 by blocking at 4 °C for four hours in Background Buster (Innovex; NB306). Samples incubated
514 with primary antibodies against neurofilament H (NF-H; EnCor; CPCA-NF-H) at 1:1,000 and
515 synaptophysin (Thermo Fisher Scientific; MA5-14532) at 1:100 diluted in 5% Background
516 Buster/1% Triton-X 100/PBS at 4 °C overnight. The muscles were then washed with PBS and
517 incubated with fluorescently conjugated secondary antibodies and Alexa Fluor 488-conjugated
518 α -bungarotoxin (Invitrogen; B13422) diluted in 5% Background Buster/PBS for two hours.

519 Images were acquired using an Olympus FLUOVIEW FV3000 confocal laser scanning
520 microscope. Complete *enface* NMJs were identified and acquired with Z-stacks using 60x and
521 100x objectives. Maximum intensity Z-stacks were reconstructed with the FV31S (Olympus)
522 software and deconvoluted with cellSens Dimension (Olympus). Blinded observers analyzed α -
523 BTX-488-labeled AChR cluster formations to determine irregularities, fragmentation, synaptic
524 size, and dispersion. Irregularities included AChR plaques, AChR perforated plaques, ring-
525 shaped or c-shaped clusters, and extensive fragmentation. Fragmentation was determined by the
526 number of identifiable individual AChR clusters within the footprint of the synapse. FUJI ImageJ
527 software was used for semi-automatic analysis of AChR clusters. Synaptic size refers to the total
528 perimeter or footprint of the postsynapse. AChR cluster dispersion was determined by the (total
529 stained area/total area) *100.

530 **Tissue biochemical analysis**

531 Mouse skeletal muscle was minced into small pieces and homogenized with polytron
532 (Kinematica, PT10-35) three times for 10 seconds at power 4 to 5 in 15 ml of TBS (150 mM
533 NaCl) with 1% TX100 and 10 mM EDTA, and protease inhibitors (per 10 mL buffer: 67 mL
534 each of 0.2 M phenylmethylsulfonylfluoride (PMSF), 0.1 M benzamidine, and 5 μ L of each of
535 leupeptin (Sigma/Millipore) 5 mg/mL, pepstatin A (Millipore) 1 mg/mL in methanol, and
536 aprotinin (Sigma-Aldrich) 5 mg/mL. The samples were incubated in a cold room 1 hr. with
537 rotation. The samples were centrifuged in a Beckman Coulter Avanti J-E centrifuge for 30
538 minutes at 20,000xg, 4 °C. The supernatant was combined with WGA slurry at 600 μ L per gram
539 of starting muscle and rotated at 4C over night.

540 The WGA beads were washed using 10X volume of WGA beads/wash 3X for three minutes at
541 1000 x g with 0.1%Tx/TBS, plus protease inhibitors. After the final wash, the WGA beads

542 (Vector Laboratories, AL-1023) were eluted with Laemmli Sample Buffer (LSB) at 600 μ L per
543 gram of starting material at 99 °C for 10 minutes. The final concentration was 1.11 mg skm/ μ L
544 beads and LSB. Samples were loaded (beads and LSB) in a 3-15% gradient gel. The proteins
545 were transferred to PVDF-FL membranes (Millipore) as previously published (*Michele et al.,*
546 *2002; Goddeeris et al., 2013*). EDTA (10 mM) was used in the homogenization to more
547 efficiently extract α -DG containing matriglycan in the muscle homogenates. (*Figure 7-figure*
548 *supplement 1 WT and POMK*), while EDTA had no effect on *myd* α -DG (matriglycan-negative)
549 extraction (*Figure 7-figure supplement 1 myd*).

550 **Immunoblotting and ligand overlay**

551 The mouse monoclonal antibody against matriglycan on α -DG (IIH6, Developmental Studies
552 Hybridoma Bank, University of Iowa; RRID:AB_2617216) was characterized previously and
553 used at 1:100 (*Ervasti and Campbell, 1991*). The polyclonal antibody, AF6868 (R&D Systems,
554 Minneapolis, MN; RRID:AB_10891298), was used at a concentration of 1:100 for
555 immunoblotting the core α -DG and β -DG proteins, and the secondary was a donkey anti-sheep
556 (LI-COR Bioscience, Lincoln, NE) used at 1:10,000 concentration. The mouse xxxx antibody
557 against matriglycan on α -DG (III HII) was previously used (*Groh et al., 2009*). Blots were
558 developed with infrared (IR) dye-conjugated secondary antibodies (*Walimbe et al., 2020*) and
559 scanned using the Odyssey infrared imaging system (LI-COR Bioscience). Blot images were
560 captured using the included Odyssey image-analysis software.

561 Laminin overlay assays were performed as previously described (*Michele et al., 2002;*
562 *Goddeeris et al., 2013*). Immobilon-FL membranes were blocked in laminin-binding buffer
563 (LBB: 10 mM triethanolamine, 140 mM NaCl, 1 mM MgCl₂, 1 mM CaCl₂, pH 7.6) containing
564 5% milk followed by incubation with mouse Engelbreth-Holm-Swarm (EHS) laminin

565 (ThermoFisher, 23017015) overnight at a concentration of 7.5 nM at 4 °C in LBB containing 3%
566 bovine serum albumin (BSA) and 2 mM CaCl₂. Membranes were washed and incubated with
567 anti-laminin antibody (L9393; Sigma-Aldrich 1:1000 dilution) followed by IRDye 800 CW dye-
568 conjugated donkey anti-rabbit IgG (LI-COR, 926–32213) at 1:10,000.

569 **Digestion of α -DG with exoglycosidases**

570 β -glucuronidase from *Thermotoga maritima* and α -xylosidase from *Sulfolobus solfataricus* were
571 cloned into pET-28a (+) vector between NheI/XhoI sites in frame with the N-terminal 6xHis tag.
572 The plasmids (20ng each) were chemically transformed into 50 μ l BL21DE3 One shot competent
573 cells. One colony each was picked and inoculated in 20ml LB (with kanamycin 50 μ g/ml)
574 overnight at 37 °C. The next day, 10 ml of the overnight culture was inoculated into 1-liter LB
575 (with kanamycin 50 μ g/ml). After reaching 0.6 OD at 600 nm the cultures were induced with 1
576 mM IPTG and incubated at 16 °C overnight. The next day the cells were centrifuged at 5000g,
577 for 10 minutes at 4 °C. Cell pellets were stored at -80 °C until ready for purification.

578 The pellets were dissolved in 20 ml homogenization buffer (50 mM Tris-Cl, 150 mM
579 NaCl, 1% TX-100, and all protease inhibitors) per liter culture. The cells were stored again
580 overnight in 50 ml falcon tubes at -80 °C for ice crystal formation. Cells were thawed the next
581 day for purification. Nuclease (Pierce) was added at 1.25kU and cells were sonicated at power
582 level four-five for four times with 10s intervals in between at 4 °C. Cells were then centrifuged at
583 15000g for 20 minutes at 4 °C. The supernatant was heat fractionated at 75 °C for 10 minutes
584 after which it was centrifuged at 15000g for 30 minutes at 4 °C. Meanwhile, a TALON
585 superflow metal affinity column was prepared by packing 3 ml of resin and equilibrating with
586 wash buffer 1 (50 mM Tris-Cl, 100 mM NaCl, 0.1% TX-100, all PIs). All further purification
587 steps were performed at 4 °C. The extract was applied to the column three times, such that each

588 time, the extract was incubated with the column for 15-30 minutes on gentle rocking platform.
589 All flowthrough was saved. The column was washed three times with wash buffer 1. All washes
590 were saved. The column was next washed with high salt wash buffer (50 mM Tris-Cl, 500 mM
591 NaCl, 0.1% TX-100, all PIs) to remove nonspecific interactions and the high salt wash was
592 saved. Proteins were then eluted with elution buffer (50 mM Tris-Cl, 100 mM NaCl, 0.1% TX-
593 100 and 300 mM Imidazole) in five fractions of three milliliters each. The relevant fractions
594 (elute 1 and 2) were pooled together, and buffer exchanged with 1XPBS pH 7.4 with 30 kDa
595 concentrators (Amicon). 100 μ l was loaded on SDS PAGE from all fractions and washes to
596 visualize with Coomassie.

597 WGA enriched glycoproteins (elutes) were buffer exchanged with Sodium acetate buffer
598 pH 5.5 using 30 kDa concentrators and heated for five minutes in the presence of 10 mM β -
599 mercaptoethanol at 99 °C. All protease inhibitors were added after the mixture cooled down. 50
600 μ l of each enzyme was added per 500 μ l of WGA-enriched and buffer-exchanged glycoproteins.
601 The initial time point was aliquoted as T₀ and the rest was incubated at 75 °C with 600 rpm
602 shaking for 16 hours.

603 **AAV vector production and AAV injection**

604 The sequence encoding mouse *like-acetylglucosaminyltransferase-1* (*Large1*) was synthesized
605 (Genscript, Piscataway, NJ) and cloned into the AAV backbone under the transcriptional control
606 of the ubiquitous CMV promoter. The AAV2/9 vector contains the genome of serotype 2
607 packaged in the capsid from serotype 9 and was selected due to its ability to improve muscle
608 transduction efficiency as well as alter tropism. The vector AAV2/9-CMV-*Large1* was generated
609 by the University of Iowa Viral Vector Core Facility. For adult mice, 100 μ L (4.35×10^{12} vg) of
610 the vector solution was administered once intraperitoneally or intravenously via the retro-orbital

611 (RO) sinus. The sequence encoding mouse *like-acetylglucosaminyltransferase-1 (Large1)* was
612 synthesized (Genscript, Piscataway, NJ) and cloned into the AAV backbone under the
613 transcriptional control of the muscle-specific MCK promoter (gift from Jeff Chamberlain). The
614 vector AAV2/9-MCK-*Large1* was generated by the University of Iowa Viral Vector Core
615 Facility. For adult mice, 100 μ L (2.55×10^{12} vg) of the vector solution were administered once
616 intraperitoneally or intravenously via the retro-orbital (RO) sinus. The sequence encoding mouse
617 *α -DG lacking the N-terminal domain (H30 – A316)* was synthesized (Genscript) and cloned into
618 the AAV backbone under the transcriptional control of the muscle-specific MCK promoter. The
619 vector AAV2/9-MCK-*DG-E* was generated by the University of Iowa Viral Vector Core
620 Facility. For adult mice, 100 μ L (6.17×10^{11} vg) of the vector solution was administered once
621 intraperitoneally or intravenously via the retro-orbital (RO) sinus. The sequence encoding mouse
622 *alpha-DG N terminal domain(α -DGN)* was synthesized (Genscript) and cloned into the AAV
623 backbone under the transcriptional control of the ubiquitous CMV promoter. The AAV2/9 vector
624 contains the genome of serotype 2 packaged in the capsid from serotype 9 and was selected due
625 to its ability to improve muscle transduction efficiency as well as alter tropism. The vector
626 AAV2/9CMV α -DGN was generated by the University of Iowa Viral Vector Core Facility. For
627 adult mice, 100 μ L (1.7×10^{12} vg) of the vector solution was administered once intraperitoneally
628 or intravenously via the retro-orbital (RO) sinus.

629 **Solid-phase assay**

630 Solid-phase assays were performed as described previously (*Michele et al., 2002; Goddeeris et*
631 *al., 2013*). Briefly, WGA N-acetyl-glycosamine buffer eluates were diluted 1:50 in TBS and
632 coated on polystyrene ELISA microplates (Costar 3590) overnight at 4 °C. Plates were washed
633 in LBB and blocked for two hours in 3% BSA/LBB at room temperature. The wells were washed

634 with 1% BSA/LBB and incubated for one hour with L9393 (1:5000 dilution) in 3% BSA/LBB
635 followed by incubation with Horseradish Peroxidase (HRP)-conjugated anti-rabbit IgG
636 (Invitrogen, 1:5000 dilution) in 3% BSA/LBB for 30 minutes. Plates were developed with o-
637 phenylenediamine dihydrochloride and H₂O₂, and reactions were stopped with 2 N H₂SO₄.
638 Absorbance per well was read at 490 nm by a microplate reader.

639 **Statistics**

640 The included Shimadzu post-run software was used to analyze LARGE1 activity in mouse
641 skeletal muscle, and the percent conversion to the product was recorded. The means of three
642 experimental replicates (biological replicates, where each replicate represents a different pair of
643 tissue culture plates or animals, i.e. control and knockout) were calculated using Microsoft
644 Excel, and the mean percent conversion to product for the WT or control sample (control mouse
645 skeletal muscle or *M-α-DGN KO* mouse skeletal muscle and myd mouse skeletal muscle,
646 respectively) reaction was set to one. The percent conversion of each experimental reaction was
647 subsequently normalized to that of the control, and statistics on normalized values were
648 performed using GraphPad Prism 8. For analysis of LARGE1 activity in mouse skeletal muscle,
649 Student's t-test was used (two-sided). Differences were considered significant at a p-value less
650 than 0.05. Graph images were also created using GraphPad Prism and the data in the present
651 study are shown as the means + / - SD unless otherwise indicated. The number of sampled units,
652 n, upon which we report statistics for *in vivo* data, is the single mouse (one mouse is n = 1).

653 **Data Availability**

654 All data generated or analyzed during this study are included in this published article.

655 **Acknowledgements**

656 We thank Keith Garringer for technical assistance and the University of Iowa Viral Vector Core
657 for generating the adeno-associated viral vector (<http://www.medicine.uiowa.edu/vectorcore>).
658 The MCK promoter was a gift from Jeff Chamberlain (University of Washington, Seattle, WA).
659 We are grateful to Dr. Jennifer Barr of the Scientific Editing and Research Communication Core
660 at the University of Iowa Carver College of Medicine for her critical reading of the manuscript.
661 We are also grateful to Amber Mower for her assistance with administrative support and Rachel
662 Poe for her support in figure design.

663 **Ethics**

664 Animal experimentation: This study was performed in strict accordance with the
665 recommendations in the Guide for the Care and Use of Laboratory Animals of the National
666 Institutes of Health. All animal experiments were approved by the Institutional Animal Care and
667 Use Committee (IACUC) protocols of the University of Iowa (#0081122).

668 **Competing Interests**

669 The authors declare no competing financial interests. Correspondence and requests for materials
670 should be addressed to K.P.C. (kevin-campbell@uiowa.edu).

671 **Funding**

672 This work was supported in part by a Paul D. Wellstone Muscular Dystrophy Specialized
673 Research Center grant (1U54NS053672 to KPC). KPC is an investigator of the Howard Hughes
674 Medical Institute. This work was also supported by the Cardiovascular Institutional Research
675 Fellowship (5T32HL007121-45 to JMH). A.S.W. is a student in the University of Iowa Medical
676 Scientist Training Program, which is funded by Medical Scientists Training Program Grant by
677 the National Institute of General Medical Sciences (NIGMS) 5 T32 GM007337.

678 **Author contributions**

679 Conceptualization: H.O., K.P.C.

680 Methodology: H.O., J.M.H, M.E.A., D.V., A.S.W., S.J., Y.H., F.S., K.M., K.P.C.

681 Formal analysis: H.O., J.M.H, M.E.A., D.V., A.S.W., S.J., K.P.C.

682 Investigation: H.O., J.M.H, M.E.A., D.V., A.S.W., S.J., Y.H., F.S., K.M., K.P.C.

683 Writing – original draft preparation: H.O., K.P.C.

684 Writing – review & editing: H.O., J.M.H, M.E.A., D.V., A.S.W., S.J., K.P.C.

685 Supervision: K.P.C.

686 Project administration: K.P.C.

687 Funding acquisition: K.P.C.

688 **Author ORCIDs**

689 Hidehiko Okuma <https://orcid.org/0000-0002-2749-9855>

690 Jeffrey M Hord <https://orcid.org/0000-0003-1343-5938>

691 Ishita Chandel <https://orcid.org/0000-00003-4821-1918>

692 Mary E Anderson <https://orcid.org/0000-0001-5342-530X>

693 David Venzke <http://orcid.org/0000-0001-8180-9562>

694 Ameya S Walimbe <https://orcid.org/0000-0002-3248-0761>

695 Soumya Joseph <https://orcid.org/0000-0002-0487-1378>

696 Zeita Gastel <https://orcid.org/0000-0003-2302-952X>

697 Yuji Hara <https://orcid.org/0000-0003-0021-1740>

698 Fumiaki Saito <https://orcid.org/0000-0002-5532-6193>

699 Kiichiro Matsumura <https://orcid.org/0000-0002-5237-8430>

700 Kevin P Campbell <https://orcid.org/0000-0003-2066-5889>

701 **References**

- 702 Brancaccio, A., Schulthess, T., Gesemann, M., Engel, J. (1995). Electron microscopic evidence
703 for a mucin-like region in chick muscle alpha-dystroglycan. *FEBS Lett*, 368(1), 139-142.
704 DOI: 10.1016/0014-5793(95)00628-m, PMID: 7615068
- 705 Carss, K. J., Stevens, E., Foley, A. R., Cirak, S., Riemersma, M., Torelli, S., Hoischen, A.,
706 Willer, T., Van Scherpenzeel, M., Moore, S. A., Messina, S., Bertini, E., Bönnemann, C.
707 G., Abdenur, J. E., Grosman, C. M., Kesari, A., Punetha, J., Quinlivan, R., Waddell, L.
708 B., Young, H. K., Wraige, E., Yau, S., Brodd, L., Feng, L., Sewry, C., MacArthur, D. G.,
709 North, K. N., Hoffman, E., Stemple, D. L., Hurles, M. E., van Bokhoven, H., Campbell,
710 K. P., Lefeber, D. J., UK10K Consortium, Lin, Y. Y., Muntoni, F. (2013). Mutations in
711 GDP-mannose pyrophosphorylase B cause congenital and limb-girdle muscular
712 dystrophies associated with hypoglycosylation of alpha-dystroglycan. *Am J Hum Genet*,
713 93(1), 29-41. DOI: 10.1016/j.ajhg.2013.05.009, PMID: 23768512
- 714 Chiba, A., Matsumura, K., Yamada, H., Inazu, T., Shimizu, T., Kusunoki, S., Kanazawa, I.,
715 Kobata, A., Endo, T. (1997). Structures of sialylated O-linked oligosaccharides of bovine
716 peripheral nerve alpha-dystroglycan. The role of a novel O-mannosyl-type
717 oligosaccharide in the binding of alpha-dystroglycan with laminin. *J Biol Chem*, 272(4),
718 2156-2162. DOI: 10.1074/jbc.272.4.2156, PMID: 8999917
- 719 Cirak, S., Foley, A. R., Herrmann, R., Willer, T., Yau, S., Stevens, E., Torelli, S., Brodd, L.,
720 Kamynina, A., Vondracek, P., Roper, H., Longman, C., Korinthenberg, R., Marrosu, G.,
721 Nürnberg, P., UK10K Consortium, Michele, D. E., Plagnol, V., Hurles, M., Moore, S. A.,
722 Sewry, C. A., Campbell, K. P., Voit, T., Muntoni, F. (2013). ISPD gene mutations are a

723 common cause of congenital and limb-girdle muscular dystrophies. *Brain*, 136(Pt 1),
724 269-281. DOI: 10.1093/brain/aws312, PMID: 23288328

725 Cohn, R. D., Henry, M. D., Michele, D. E., Barresi, R., Saito, F., Moore, S. A., Flanagan, J. D.,
726 Skwarchuk, M. W., Robbins, M. E., Mendell, J. R., Williamson, R. A., Campbell, K. P.
727 (2002). Disruption of DAG1 in differentiated skeletal muscle reveals a role for
728 dystroglycan in muscle regeneration. *Cell*, 110(5), 639-648. DOI: 10.1016/s0092-
729 8674(02)00907-8, PMID: 12230980

730 de Greef, J. C., Hamlyn R., Jensen B. S., Ocampo Landa, R., Levy J. R., Kobuke K., Campbell
731 K. P. (2016). Collagen VI deficiency reduces muscle pathology, but does not improve
732 muscle function, in the γ -sarcoglycan-null mouse. *Human Molecular Genetics*. 25(7),
733 1357-1369. DOI: 10.1093/hmg/ddw018, PMID: 26908621

734 de Greef, J. C., Slutter, B., Anderson, M. E., Hamlyn, R., O'Campo Landa, R., McNutt, E. J.
735 Hara, Y., Pewe, L. L., Venzke, D., Matsumura, K., Saito, F., Harty, J. T., Campbell, K. P.
736 (2019). Protective role for the N-terminal domain of alpha-dystroglycan in Influenza A
737 virus proliferation. *Proc Natl Acad Sci U S A*, 116(23), 11396-11401. DOI:
738 10.1073/pnas.1904493116, PMID: 31097590

739 Dong, M., Noguchi, S., Endo, Y., Hayashi, Y. K., Yoshida, S., Nonaka, I., Nishino, I. (2015).
740 DAG1 mutations associated with asymptomatic hyperCKemia and hypoglycosylation of
741 alpha-dystroglycan. *Neurology*, 84(3), 273-279. DOI: 10.1212/WNL.0000000000001162,
742 PMID: 25503980

743 Ervasti, J. M., & Campbell, K. P. (1993). A role for the dystrophin-glycoprotein complex as a
744 transmembrane linker between laminin and actin. *J Cell Biol*, 122(4), 809-823. DOI:
745 10.1083/jcb.122.4.809, PMID: 8349731

- 746 Goddeeris, M. M., Wu, B., Venzke, D., Yoshida-Moriguchi, T., Saito, F., Matsumura, K.,
747 Moore, S. A., Campbell, K. P. (2013). LARGE glycans on dystroglycan function as a
748 tunable matrix scaffold to prevent dystrophy. *Nature*, 503(7474), 136-140. DOI:
749 10.1038/nature12605, PMID: 24132234
- 750 Groh S, Zong H, Goddeeris MM, Lebakken CS, Venzke D, Pessin JE, Campbell KP.
751 Sarcoglycan complex: implications for metabolic defects in muscular dystrophies. *J Biol*
752 *Chem*. 2009 Jul 17;284(29):19178-82. doi: 10.1074/jbc.C109.010728. Epub 2009 Jun 3.
753 PMID: 19494113; PMCID: PMC2740540.
- 754 Han, R., Kanagawa, M., Yoshida-Moriguchi, T., Rader, E., Ng., R.A., Michele, D.E., Muirhead,
755 D.E., Kunz, S., Moore, S.A., Iannaccone, S.T., Miyake, K., McNeil, P.L., Mayer, U.,
756 Oldstone, M.B.A., Faulkner, J.A. and Campbell, K.P. (2009). Basal Lamina Strengthens
757 Cell Membrane Integrity via the Laminin G Domain Binding of α -Dystroglycan. *Proc.*
758 *Natl. Acad. Sci. U.S.A.* 106(31), 12573-12579. DOI: 10.1073/pnas.0906545106, PMID:
759 19633189
- 760 Hara, Y., Balci-Hayta, B., Yoshida-Moriguchi, T., Kanagawa, M., Beltran-Valero de Bernabe,
761 D., Gündesli, H., Willer, T., Satz, J. S., Crawford, R. W., Burden, S. J., Kunz, S.,
762 Oldstone, M. B. A., Accardi, A., Talim, B., Muntoni, F., Topaloğlu, H., Dinçer, P.,
763 Campbell, K. P. (2011). A dystroglycan mutation associated with limb-girdle muscular
764 dystrophy. *N Engl J Med*, 364(10), 939-946. DOI: 10.1056/NEJMoa1006939, PMID:
765 21388311
- 766 Hara, Y., Kanagawa, M., Kunz, S., Yoshida-Moriguchi, T., Satz, J. S., Kobayashi, Y. M., Zhu,
767 Z., Burden, S. J., Oldstone, M. B. A., Campbell, K. P. (2011). Like-
768 acetylglucosaminyltransferase (LARGE)-dependent modification of dystroglycan at Thr-

769 317/319 is required for laminin binding and arenavirus infection. *Proc Natl Acad Sci U S*
770 *A*, 108(42), 17426-17431. DOI: 10.1073/pnas.1114836108, PMID: 21987822

771 Henry, M. D. and Campbell, K. P. (1998) A Role for Dystroglycan in Basement Membrane
772 Assembly. *Cell*, 95(6), 859-870. DOI: 10.1016/s0092-8674(00)81708-0, PMID: 9865703

773 Hohenester, E. (2019). Laminin G-like domains: dystroglycan-specific lectins. *Curr Opin Struct*
774 *Biol*, 56, 56-63. DOI: 10.1016/j.sbi.2018.11.007, PMID: 30530204

775 Ibraghimov-Beskrovnya, O., Ervasti, J. M., Leveille, C. J., Slaughter, C. A., Sernett, S. W.,
776 Campbell, K. P. (1992). Primary structure of dystrophin-associated glycoproteins linking
777 dystrophin to the extracellular matrix. *Nature*, 355(6362), 696-702. DOI:
778 10.1038/355696a0, PMID: 1741056

779 Inamori, K., Yoshida-Moriguchi, T., Hara, Y., Anderson, M. E., Yu, L., Campbell, K. P. (2012).
780 Dystroglycan Function Requires Xylosyl- and Glucuronyltransferase Activities of
781 LARGE. *Science*, 335(6064), 93-96. DOI: 10.1126/science.1214115, PMID: 22223806

782 Jung, D., Yang, B., Meyer, J., Chamberlain, J. S., Campbell, K. P. (1995). Identification and
783 characterization of the dystrophin anchoring site on beta-dystroglycan. *J Biol Chem*,
784 270(45), 27305-27310. DOI: 10.1074/jbc.270.45.27305, PMID: 7592992

785 Kanagawa, M., Nishimoto, A., Chiyonobu, T., Takeda, S., Miyagoe-Suzuki, Y., Wang, F.,
786 Fujikake, N., Taniguchi, M., Lu, Z., Tachikawa, M., Nagai, Y., Tashiro, F., Miyazaki, J.,
787 Tajima, Y., Takeda, S., Endo, T., Kobayashi, K., Campbell, K. P., Toda, T. (2009).
788 Residual laminin-binding activity and enhanced dystroglycan glycosylation by LARGE
789 in novel model mice to dystroglycanopathy. *Hum Mol Genet*, 18(4), 621-631. DOI:
790 10.1093/hmg/ddn387, PMID: 19017726

791 Kanagawa, M., Saito, F., Kunz, S., Yoshida-Moriguchi, T., Barresi, R., Kobayashi, Y. M.,
792 Muschler, J., Dumanski, J. P., Michele, D. E., Oldstone, M. A. B., Campbell, K. P.
793 (2004). Molecular recognition by LARGE is essential for expression of functional
794 dystroglycan. *Cell*, *117*(7), 953-964. DOI: 10.1016/j.cell.2004.06.003, PMID: 15210115

795 Lane, P. W., Beamer, T. C., Myers, D. D. (1976). Myodystrophy, a new myopathy on
796 chromosome 8 of the mouse. *J. Hered.* **67**, 135-138. DOI:
797 10.1093/oxfordjournals.jhered.a108687, PMID: 939913

798 Michele, D. E., Barresi, R., Kanagawa, M., Saito, F., Cohn, R. D., Satz, J. S., Dollar, J., Nishino,
799 I., Kelley, R. I., Somer, H., Straub, V., Mathews, K. D., Moore, S. A., Campbell, K. P.
800 (2002). Post-translational disruption of dystroglycan-ligand interactions in congenital
801 muscular dystrophies. *Nature*, *418*(6896), 417-422. DOI: 10.1038/nature00837, PMID:
802 12140558

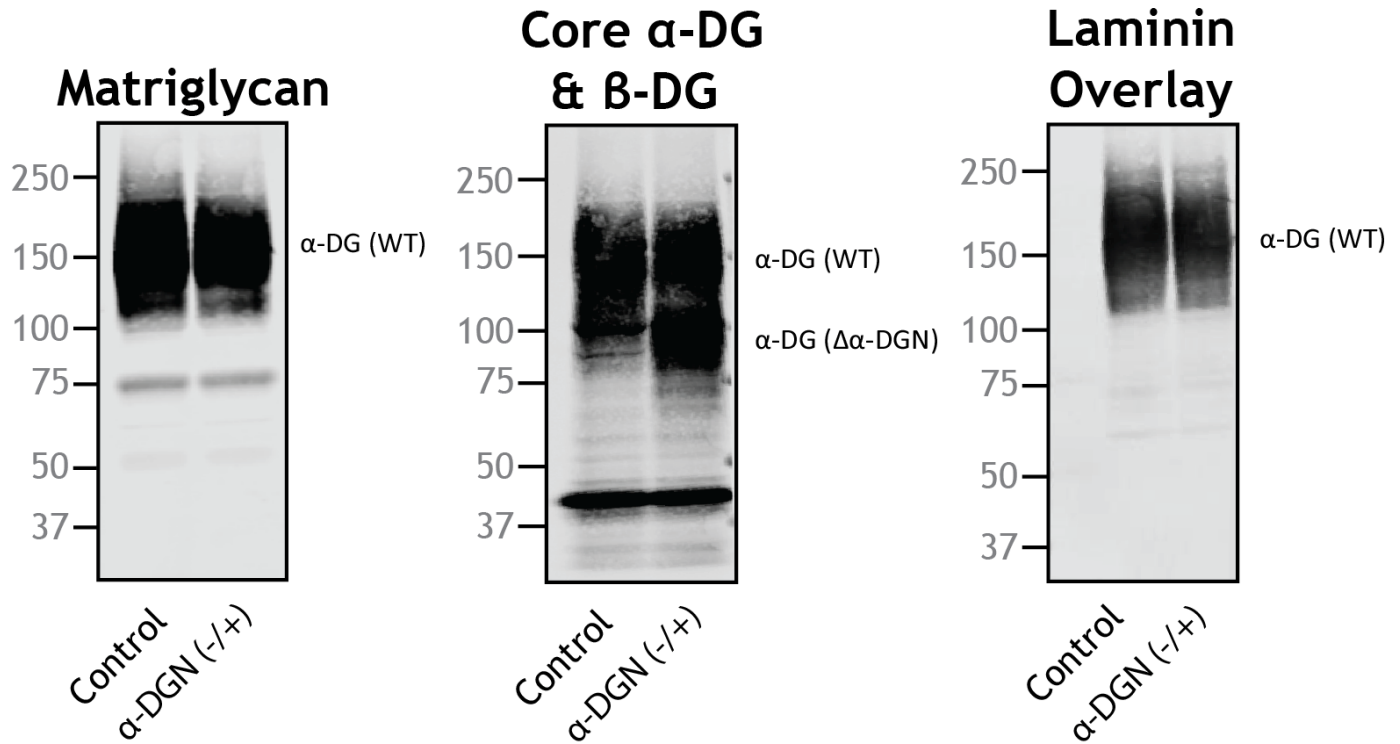
803 Nishimune, H., Valdez, G., Jarad, G., Moulson, C. L., Müller, U., Miner, J. H., & Sanes, J. R.
804 (2008). Laminins promote postsynaptic maturation by an autocrine mechanism at the
805 neuromuscular junction. *Journal of Cell Biology*, *182*(6), 1201–1215. DOI:
806 10.1083/jcb.200805095

807 Ohtsubo, K., & Marth, J. D. (2006). Glycosylation in cellular mechanisms of health and disease.
808 *Cell*, *126*(5), 855-867. DOI: 10.1016/j.cell.2006.08.019, PMID: 16959566

809 Puckett, R. L., Moore, S. A., Winder, T. L., Willer, T., Romansky, S. G., Covault, K. K.,
810 Campbell, K. P., Abdenur, J. E. (2009). Further evidence of Fukutin mutations as a cause
811 of childhood onset limb-girdle muscular dystrophy without mental retardation.
812 *Neuromuscul Disord*, *19*(5), 352-356. DOI: 10.1016/j.nmd.2009.03.001, PMID:
813 19342235

- 814 Rowe., R. G., Weiss, S. J. (2008). Breaching the basement membrane: who, when, and how?
815 *Trends in Cell Biology*, 18(11), 560-574. DOI: 10.1016/j.tcb.2008.08.007. Epub 2008 Oct
816 9. PMID: 18848450.
- 817 Saito, F., Moore, S. A., Barresi, R., Henry, M. D., Messing, A., Ross-Barta, S. E., Cohn, R. D.,
818 Williamson, R. A., Sluka, K. A., Sherman, D. L., Brophy, P. J., Schmelzer, J. D., Low, P.
819 A., Wrabetz, L., Feltri, M. L., Campbell, K. P. (2003). Unique role of dystroglycan in
820 peripheral nerve myelination, nodal structure, and sodium channel stabilization. *Neuron*,
821 38(5), 747-758. DOI: 10.1016/s0896-6273(03)00301-5, PMID: 12797959
- 822 Suzuki, A., Yoshida, M., Hayashi, K., Mizuno, Y., Hagiwara, Y., Ozawa, E. (1994). Molecular
823 organization at the glycoprotein-complex-binding site of dystrophin. Three dystrophin-
824 associated proteins bind directly to the carboxy-terminal portion of dystrophin. *Eur J*
825 *Biochem*, 220(2), 283-292. DOI: 10.1111/j.1432-1033.1994.tb18624.x, PMID: 8125086
- 826 Walimbe, A. S., Okuma, H., Joseph, S., Yang, T., Yonekawa, T., Hord, J. M., Venzke, D.,
827 Anderson, M. E., Torelli, S., Manzur, A., Devereaux, M., Cuellar, M., Prouty, S.,
828 Ocampo Landa, S., Yu, L., Xiao, J., Dixon, J. E., Muntoni, F., Campbell, K. P. (2020).
829 POMK regulates dystroglycan function via LARGE1-mediated elongation of
830 matriglycan. *Elife*, 9. DOI: 10.7554/eLife.61388, PMID: 32975514
- 831 Williamson, R. A., Henry, M. D., Daniels, K. J., Hrstka, R. F., Lee, J. C., Sunada, Y.,
832 Ibraghimov-Beskrovnaya, O., Campbell, K. P. (1997). Dystroglycan is essential for early
833 embryonic development: disruption of Reichert's membrane in Dag1-null mice. *Hum Mol*
834 *Genet*, 6(6), 831-841. DOI: 10.1093/hmg/6.6.831, PMID: 9175728

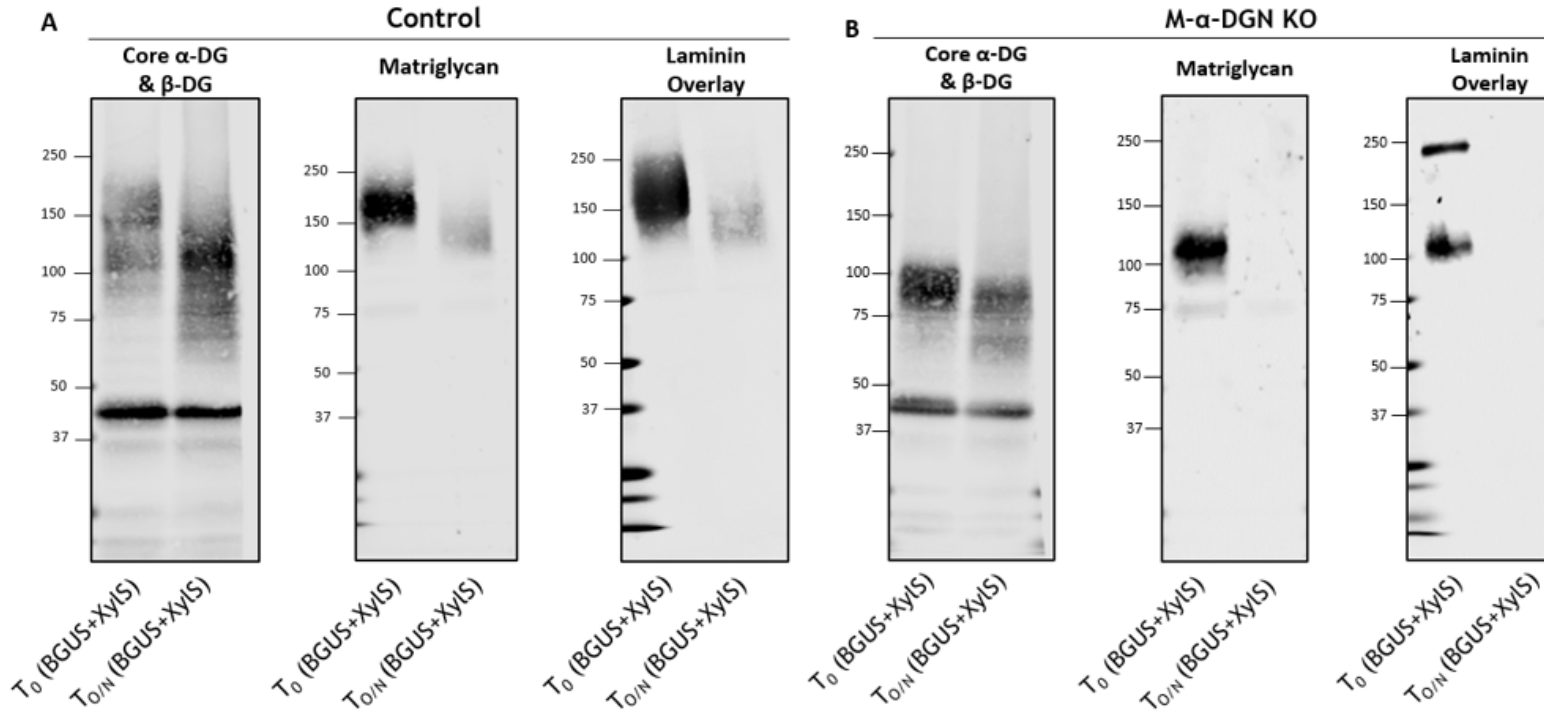
- 835 Yoshida-Moriguchi, T., & Campbell, K. P. (2015). Matriglycan: a novel polysaccharide that
836 links dystroglycan to the basement membrane. *Glycobiology*, 25(7), 702-713. DOI:
837 10.1093/glycob/cwv021, PMID: 25882296



838 **Supplemental Figures**

839

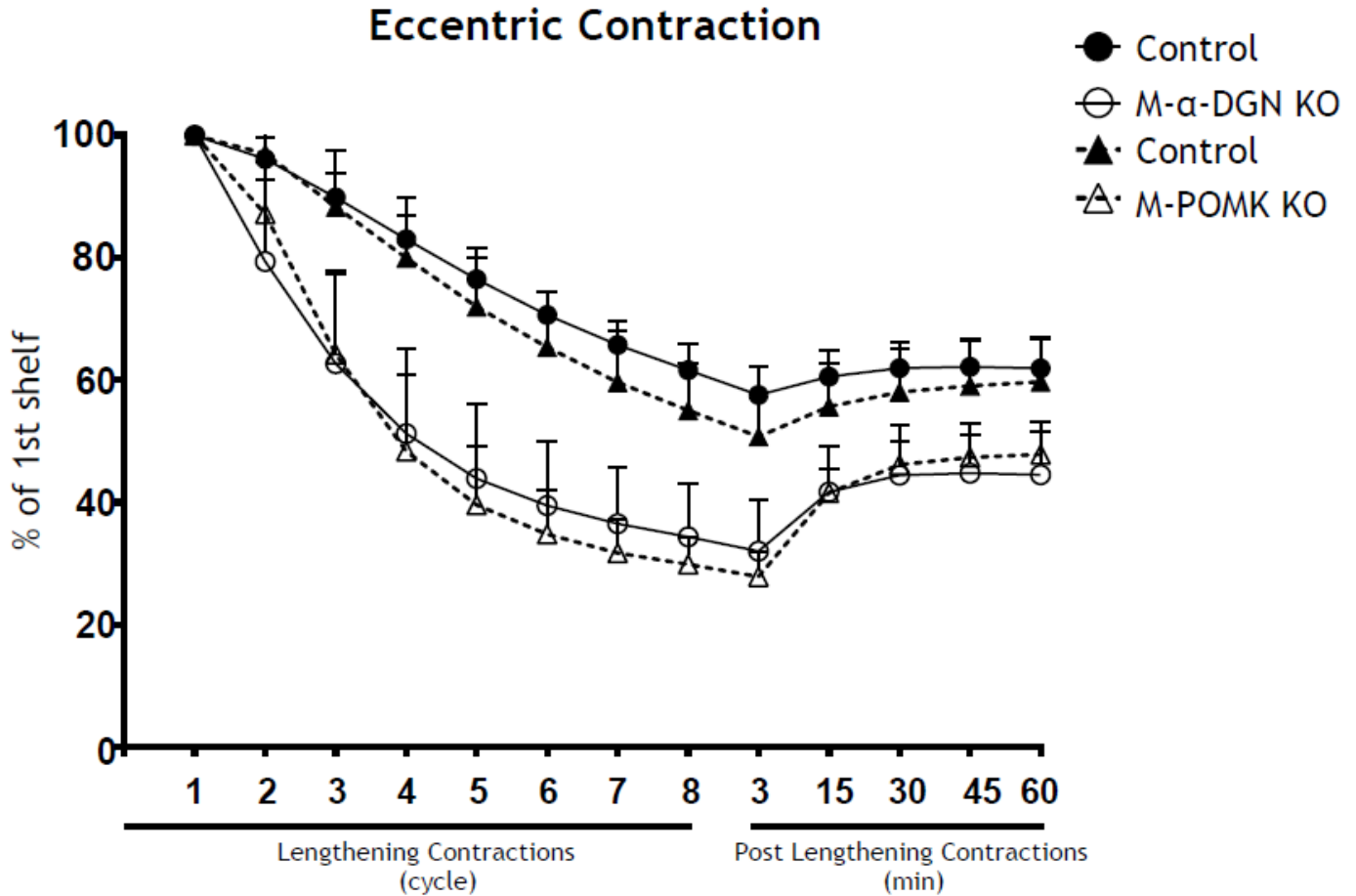
840 **Figure 2-figure supplement 1. Heterozygous mice (+/-) for constitutive deletion of α-DGN**
841 **have two different sizes of α-DG** Immunoblot analysis of skeletal muscle from littermate
842 controls or mice that were heterozygous for the α-DGN KO allele (α-DGN (-/+)). Glycoproteins
843 were enriched from quadriceps skeletal muscles of mice using WGA-agarose with 10 mM
844 EDTA. Immunoblotting was performed to detect matriglycan (IIIH11), core α-DG and β-DG
845 (AF6868), and laminin overlay. α-DG in WT control muscle (α-DG(WT)) and α-DG in α-DGN-
846 deficient muscle (α-DG(Δα-DGN)) are indicated on the right. Molecular weight standards in
847 kilodaltons (kDa) are shown on the left.



848

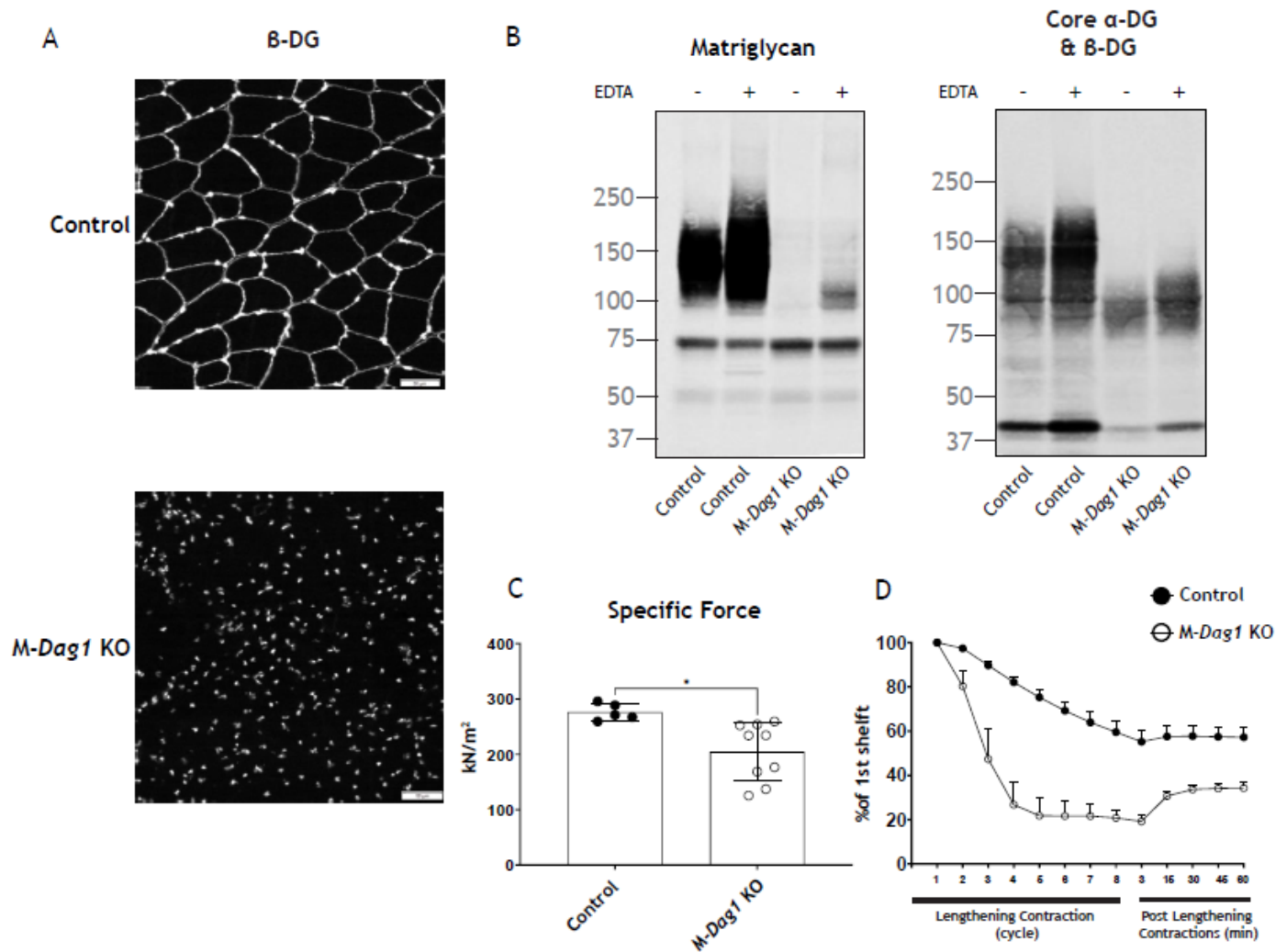
849 **Figure 2-figure supplement 2. The short 100-120kDa band in M- α -DGN KO is matriglycan.**

850 (A) Immunoblot analysis of total skeletal muscle from control mice after digestion with enzymes
851 β -glucuronidase and α -xylosidase. Glycoproteins were enriched using wheat-germ agglutinin
852 (WGA)-agarose with 10 mM EDTA and incubated overnight with β -glucuronidase (BGUS) and
853 α -xylosidase (XylS). Immunoblotting was performed to detect matriglycan (IIH6), core α -DG
854 and β -DG (AF6868), and laminin overlay before (T_0) and after overnight digestion ($T_{0/N}$). (B)
855 Immunoblot analysis of M- α -DGN KO total skeletal muscle after digestion with enzymes β -
856 glucuronidase and α -xylosidase. Glycoproteins were enriched using wheat-germ agglutinin
857 (WGA)-agarose with 10 mM EDTA and incubated overnight with β -glucuronidase and α -
858 xylosidase. Immunoblotting was performed to detect matriglycan (IIH6), core α -DG and β -DG
859 (AF6868), and laminin overlay before (T_0) and after digestion ($T_{0/N}$). Molecular weight
860 standards in kilodaltons (kDa) are shown on the left.

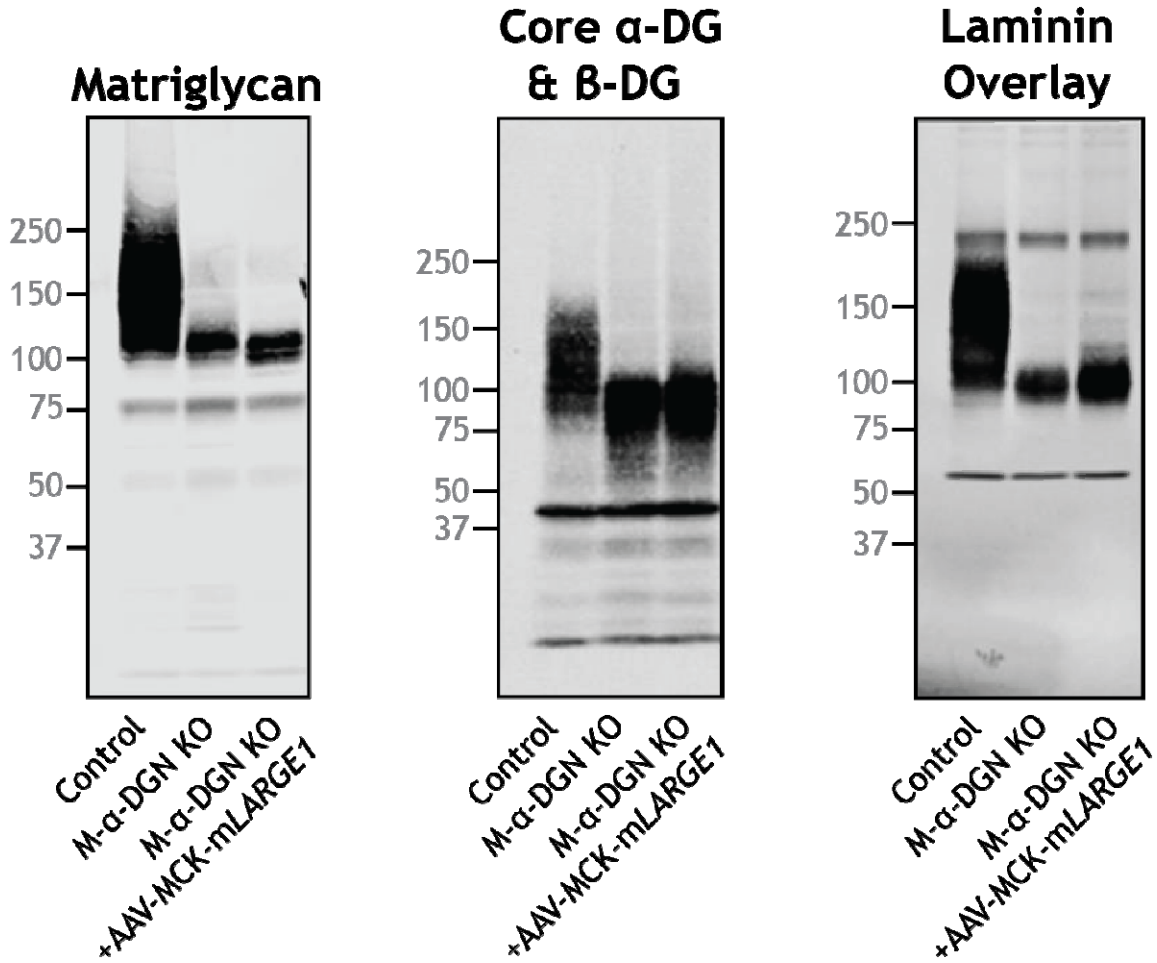


861

862 **Figure 4-figure supplement 1. α -DGN-deficient muscle and POMK-deficient muscle with**
863 **similar short forms of matriglycan exhibit similar lengthening contraction-induced force**
864 **decline.** Force deficit and force recovery after eccentric contractions in EDL muscles from 12- to
865 17-week-old male & female controls (closed circles; n=7), M- α -DGN KO (open circles; n=7),
866 M-POMK littermate controls (closed triangles; n=3), and M-POMK KO (open triangles; n=4)
867 mice. There is no significant difference in M- α -DGN KO vs M-POMK KO as determined by
868 Student's unpaired t-test at any given lengthening contractions cycle and post lengthening
869 contractions.

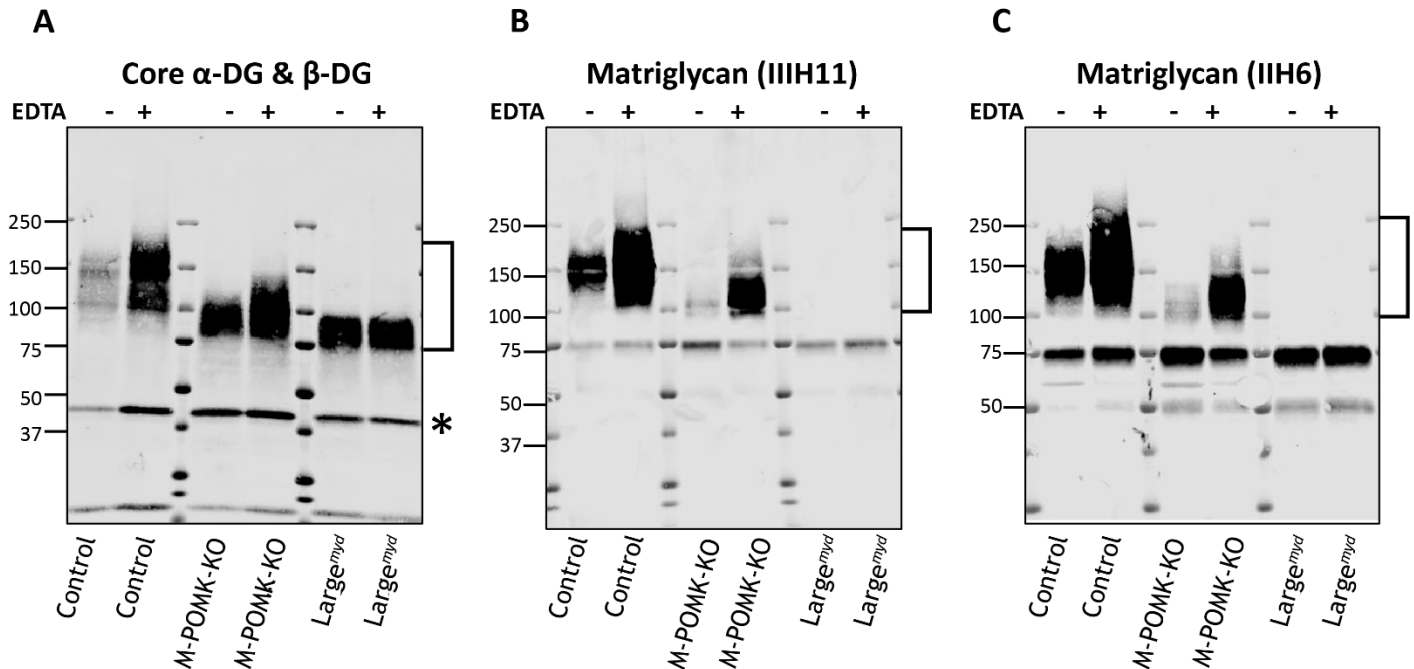


870
 871 **Figure 5-figure supplement 1. Characteristics of M-Dag1 KO (*Pax7^{cre} Dag1^{flx/flx}*) mice (A)**
 872 Immunofluorescence analyses of quadriceps muscles from a 12-week-old WT littermate
 873 (control) or M-Dag1 KO mouse. Sections were stained to detect β-DG (AP83) and nuclei
 874 (DAPI). (B) Immunoblot analysis of skeletal muscle from control and M-Dag1 KO mice.
 875 Glycoproteins were enriched from skeletal muscles (quadriceps) using WGA-agarose with (+)
 876 and without (-) 10 mM EDTA. Immunoblotting was performed to detect matriglycan (IIIH11)
 877 and core α-DG and β-DG (AF6868). (C) Specific force in EDL muscles of mice in indicated
 878 groups; p=0.0128, as determined by Student's unpaired t-test. (D) Force deficit and force
 879 recovery after eccentric contractions in EDL muscles of 12- to 17-week-old male & female
 880 control (n=3) and M-Dag1 KO (n=6) mice.



881

882 **Figure 6-figure supplement 1. LARGE1 overexpression does not extend matriglycan on**
883 **dystroglycan lacking α -DGN.** AAV-MCK-LARGE1 was injected into the retro-orbital sinus 10-
884 to-24-week-old M- α -DGN KO mice. Quadriceps skeletal muscle was dissected 10 to 22 weeks
885 after injection from control, M- α -DGN KO, and M- α -DGN KO+AAV-MCK-mLARGE1 and
886 used for immunoblotting analysis. Glycoproteins were enriched using WGA-agarose with 10
887 mM EDTA. Immunoblotting was performed to detect matriglycan (IIIH11), core α -DG and β -
888 DG (AF6868), and laminin (overlay). Molecular weight standards in kilodaltons (kDa) are
889 shown on the left.



890

891 **Figure 7-figure supplement 1. Effect of EDTA on solubilization of α -DG from skeletal**
892 **muscle.** Western blot analysis of DG in glycoprotein-enriched samples of control, M-POMK-
893 KO, and *Large^{myd}* skeletal muscle. Homogenates were prepared with (+) and without (-) 10mM
894 EDTA (indicated on top) and enriched on WGA-agarose beads. Following washing, WGA-
895 agarose beads were eluted with Laemmli sample buffer, and samples were loaded onto SDS-
896 PAGE and blotted onto PVDF-FL membranes. Immunoblotting was performed to detect (A)
897 core α -DG & β -DG (AF6868), (B) matriglycan (IIIH11) and (C) matriglycan (IIH6). α -DG is
898 labeled with a bracket and varies in apparent molecular weight depending on glycosylation with
899 matriglycan. β -DG is labeled with an asterisk.